공학박사학위논문

DC impedance-based Flow Cytometry on a Microfluidic Chip for Detection of Circulating Tumor Cell and Submicron-sized Bacteria

순환 암세포와 박테리아 검출을 위한 직류 전기저항 기반 유동세포계수 미세유체칩

2014년 8월

서울대학교 대학원
협동과정 바이오엔지니어링 전공
최 형 선

Ph.D. Dissertation

DC impedance-based Flow Cytometry on a Microfluidic Chip for Detection of Circulating Tumor Cell and Submicron-sized Bacteria

BY

HYOUNGSEON CHOI

AUGUST 2014

INTERDISCIPLINARY PROGRAM FOR
BIOENGINEERING THE GRADUATE SCHOOL
SEOUL NATIONAL UNIVERSITY

ABSTRACT

DC impedance-based Flow Cytometry on a Microfluidic Chip for Detection of Circulating Tumor Cell and Submicron-sized Bacteria

Hyoungseon Choi
Interdisciplinary Program for Bioengineering
The Graduate School
Seoul National University

This dissertation is focused on a miniaturized flow cytometry platform based on a microfluidic chip and practical applications for circulating tumor cell and submicron-sized bacteria using the platform. Flow cytometry is a conventional and attractive technology to analyze various features of single cells (or particles) and to count the number of cells (or particles). With increasing needs for flow

cytometry as a point-of-care testing (POCT) device in clinical and biochemical fields, cheap and easy to operate miniaturized flow cytometry platform has been developed worldwide. Especially with the microfabrication technology innovation, microfluidic system-based flow cytometry platform is very attractive in a multidisciplinary field of biochemistry, nanotechnology, biotechnology, mechanical engineering, and electrical engineering due to small volumes of sample, low-costs, small system size, and fast analysis time. In this work, the author shows a developed DC impedance-based micro flow cytometer and its applications as a circulating tumor cell (CTC) counter and a bacteria detection system.

First, the author described a simple, label-free, and efficient DC impedance-based microcytometer for CTC detection. Although there have been many CTC detection approaches, most methods were based on immunoreaction with epithelial cell adhesion molecule (EpCAM), because it is well-known that EpCAM is the most common proteins on CTCs. However, recent researches showed that their EpCAM were lost by epithelial-mesenchymal transition (EMT) process, and some leukocytes have EpCAM on their surfaces. Therefore, the author utilized morphological features of CTCs; larger size than normal peripheral blood cells such RBCs and WBCs. The

proposed DC impedance-flow cytometer rapidly measured the size of every cells based on the DC impedance peak amplitudes. With the developed micro flow cytometer, the author tested spiked ovarian cancer cells in normal blood samples and real breast cancer patient blood samples, resulting in a high efficiency of ~88 % and all positive signs from all patient samples. This results prove that the developed device has a potential to be a portable and daily healthcare device for cancer diagnosis and prognosis.

Secondly, the author presented flow cytometry-based submicron-sized bacteria detection system using movable virtual wall. For water quality tests, many bacterial detection approaches have been used everywhere. Conventional bacterial detection methods are labor-intensive and time-consuming. In addition, highly-trained experts are needed to exam. To overcome those limitations, the author suggested a miniaturized flow cytometry-based bacterial detection system with a virtual wall using non-conducting solution. The proposed system basically utilize DC impedance-based detection method to measure the size of bacteria and to know the presence and fluorescence-based detection method to recognize the kind of bacteria. In addition, to detect very small ranging submicron to 4 μm-sized cells, the author introduce an adjustable virtual wall with

non-conducting solution. Because virtual wall solution has no ions and does not mix with sample solution due to laminar flow, it behaves like channel wall. With the developed system, the author detected 0.99, 1.69 and 4.16 μm-sized microparticles and submicron-sized bacteria; *F. tularensis*. In addition, the micro cytometer distinguish *F. tularensis* and *E. coli* with DC impedance and fluorescence successfully. From these results, developed cytometry-based bacterial sensor is a facile, sensitive, accurate and fast means of bacterial detection.

Keywords : Microfluidic system, flow cytometry, DC impedance detection, fluorescence detection, circulating tumor cell (CTC), bacterial detection

Student Number : 2009-21079

CONTENTS

Abstract ····· i

Contents ····· v

List of Figures and Tables ····· ix

Chapter 1. ····· 1

Introduction

1.1. Flow cytometry ····· 2

1.2. Miniaturized Flow Cytometry-based Cell Detection System on a Microfluidic Chip

1.2.1. Microfluidic System ····· 6

1.2.2. Importance of Miniaturized Flow Cytometry System ····· 7

1.2.3. Approaches for Flow Cytometer-based Cell Detection System on a Microfluidic Chip ····· 8

1.3. Goals of Study ····· 16

Chapter 2. ····· 18

A label-free DC impedance-based microcytometer for circulating rare cancer cell counting

2.1. Introduction

2.1.1. Circulating Tumor Cells (CTCs) ····· 19

2.1.2. Approaches for Counting CTCs

2.1.2.1 Conventional Approaches ····· 21

2.1.2.2 Microfluidic chip-based approaches ····· 25

2.1.3 Goals of Study ····· 27

2.2. System Scheme ····· 28

2.3. Experimental Method

2.3.1. Sample Preparation ····· 31

2.3.2. Experimental Setup ····· 33

2.4. Results and Discussion

2.4.1. System Calibration ····· 34

2.4.2. Size Distribution of Ovarian Cancer Cells ····· 38

2.4.3. Counting Efficiency of Rare Cells in Blood ····· 40

2.4.4. Patient Sample Test ····· 44

2.5. Conclusion and Perspective ····· 48

2.6. Further Study ····· 49

Chapter 3. ····· 51

Flow cytometry-based submicron-sized bacterial detection system using movable virtual wall

3.1. Introduction

3.1.1. Importance of Bacteria Detection ····· 52

3.1.2. Approaches for Bacteria Detection ····· 52

3.1.3. Goals of Study ····· 57

3.2. System Scheme ····· 57

3.3. Experimental Method

3.3.1. Sample Preparation ····· 61

3.3.2. Simulation ····· 62

3.3.3. Experimental Setup ····· 64

3.4. Results and Discussion

3.4.1. Simulation ····· 65

3.4.2. Detection of Changes in DC impedance and Fluorescence · 66

3.4.3. Effect of the Movable Virtual Wall ····· 68

3.4.4. Bacterial Detection ····· 74

3.5. Conclusion and Perspective ····· 79

Chapter 4. ····· 81

Conclusion and Perspective

Bibliography ····· 85

Appendix

A. Chip Fabrication ····· 99

B. Polyelectrolytic Gel Electrode (PGE) Fabrication ····· 102

C. System parallelization plan ····· 103

국문초록 ····· 104

List of Figures and Tables

Figure 1-1. Coulter counter diagram with the Coulter principles. A beaker contains microparticles suspended in electrolytic solution and microparticles move through a small aperture on a chamber wall by pump. Two electrodes, one inside and the other one outside an aperture tube, are electrically connected by an ionic flow and measure the impedance change when a particle pass through an aperture. (Beckman Coulter, Inc.)

Figure 1-2. Schematic view of optical detection based-flow cytometry. (a) Cells (or particles) flow through the fluid stream and pass by a focused laser beam. By laser beam, fluorescence chemicals on/in a cell get excited and emit the fluorescence. Fluorescence light will be divided into multi-wavelength by various filters and detected by the photon detector such as PMT. (Semrock, Inc.) (b) When a particle is passing the laser beam, Laser beam will be scattered in some ways; FSC and SSC. (c) The intensity of the fluorescence (or scattered lights) are plotted on graphs.

Figure 1-3. Optical detection based-micro flow cytometer system. (a) PDMS-based opto-fluidic micro flow cytometer embedded optical fibers into the microfluidic chip. (b) Packaged microfluidic flow cytometer. (c) Schematic set-up for fluorescence detection-based micro cytometer and cell sorter. (d) Layered structure of the device with the input and output waveguides, lens system, and microchannel as well as light rays.

Figure 1-4. Impedance detection-based micro flow cytometer system. (a) The metal electrode patterned microfabricated chip with a PDMS cover and molded fluidic connections. (b) Schematic diagram of the microfluidic AC impedance cytometer using a differential detection. (c) DC impedance analysis with the polyelectrolytic salt bridge-based electrode. (d) Microfluidic glass chip with one pair of polymer.

Figure 1-5. Micro flow cytometer system using simultaneous detection of fluorescence and impedance. (a) The cytometer chip with micro-electrodes for impedance spectroscopy (AC impedance) and the different grooves for holding fibers (excitation source and emission paths).

(b) Schematic diagram for microfluidic cytometer using DC impedance detection and fluorescence detection with LED and SSPM as a light source and detector, respectively. (c) Pictures of the completed microfluidic cytometer.

Figure 2-1. (a) From a primary tumor, a subpopulation of cells are detached and propagate into blood circulation. Cells that enter into the blood vessel, which is called circulating tumor cells (CTCs), survive in the circulation and attach to the secondary site, which can grow to secondary tumors. (b) Kaplan-Meier plot shows a relationship between the probability of survival and the time. From the plot, the number of CTCs affect to the survival rates [25].

Figure 2-2. Conventional approaches for CTC detection (a) CellSearch system (Veridex, NJ). (b) The principle of ISET (Isolation by Size Epthelial Tumor cells). (c) Process to separate CTCs by RosetteSep^{TM}.

Figure 2-3. (a) Schematic illustration of the DC impedance-based cell counter. Ionic flows between the PGEs under low DC bias (b) are interrupted when a cell passes through,

causing a DC impedance change (c). (d) Film mask image for the microfluidic chip and the enlarged image of detection region. A photograph of the microfluidic glass chip (e) equipped with a fluidic connection with NanoPort Assemblies (Upchurch) (f). (g) Enlarged image of the detection region in the fabricated microfluidic glass chip. The main channel is 70 μm wide and 25 μm high.

Figure 2-4. (a) Calibration curve of the impedance peak amplitude corresponding to the volumes of 8.31, 10.35, and 15.02 μm diameter particles. Standard error bars are from five independent experiments. (b) Histogram of the impedance peak amplitude obtained from various microbeads, WBCs, and ovarian cancer cell lines (OVCAR-3). The WBCs were fluorescently labelled using a CD45 antibody, and the impedance peaks that synchronize with fluorescent peaks were counted.

Figure 2-5. Schematics for normal blood cells (a) and a cancer cell (b) in blood samples flowing through microchannels. In (a), RBCs occupy about 45 % of the volume of one CTC with a diameter of *d*. Other minor blood cells are

ignored.

Figure 2-6. Simultaneous impedance and fluorescence signals from normal blood samples of healthy volunteers (a), and from OVCAR-3 cells spiked into normal blood (b) after labeling with EpCAM antibody. In (b), the peaks over the impedance threshold (0.4) synchronize with fluorescence peaks. (c) The counting efficiency is about 88 % and is linear over the entire range under the optimal flow rate (R2 = 0.999) when a range of cells (10, 100, 500, and 1000 cells) was spiked in healthy normal blood samples. Standard error bars are from five independent experiments. Light (d) and fluorescence (e) images of EpCAM-labeled OVCAR-3 cancer cells spiked into blood. Scale bar = 20 μm.

Figure 2-7. Detection of CTCs from blood samples (500 μl) of breast cancer patients in stage Ⅳ. (a) Simultaneous measurement of fluorescence and impedance signals from patient blood stained with Her2 antibody. The peaks in broken lines indicate cells with Her2 positive but below the impedance threshold. (b) Impedance peaks over the threshold value were detected and counted in

all of the 24 blood samples from patients, whereas no such peaks were detected in blood samples from 5 healthy donors. In two out of three blood samples from patients who have finished chemotherapy treatment, no impedance peaks over the impedance threshold were detected. (c) Representative impedance signals from the 22nd patient sample.

Figure 3-1. Conventional approaches for bacteria detection system. (a) Colony counting method. (b) Polymerase chain reaction (PCR)-based method.

Figure 3-2. Various bacteria detection system. (a) Scheme of the microfluidic system, which consists of microchannels for bacteria immunocaptured with magnetic particles, and gold electrodes for reduction of enzyme-produced *p*-benzoquinone (BQ). (b) Schematic view of the Hartman interferometer. A single planar wave of linearly polarized light is coupled into a thin waveguiding layer. (c) CMOS biochip immunosensor for detection of a single bacteria.

Figure 3-3. (a) Schematic illustration of the flow cytometry-based submicron-sized bacterial detection system. (b) A virtual

wall solution with a slow flow rate, although enabling detection of large particles, renders a relatively low current density and a wide channel width, preventing detection of submicron particles. (c) Fast flow of the wall solution narrows the channel, yielding higher current density and thus greater DC impedance change (ΔZ) required for detection of submicron particles (figures not drawn to scale).

Figure 3-4. (a) Mask pattern of the microfluidic chip for the flow cytometry-based submicron-sized bacterial detection system. (b) Photographs of the detection region in the fabricated microfluidic glass chip (scale bar = 100 μm). (c) Illustration of varing thickness of the detection area (gray) obtained by controlling the flow rate of the virtual wall (black).

Figure 3-5. Simulation results of the current density (A m^{-2}) obtained by applying a 1 V DC voltage to a pair of electrodes (a) without and (b) with the virtual wall.

Figure 3-6. Representative profile of simultaneous detection of DC impedance changes (ΔZ) and fluorescence signals from 4.16 μm diameter polymer particles The fluorescence

peak lies in between the biphasic ΔZ peaks.

Figure 3-7. (a) The effective channel width as a function of the flow rate of virtual wall solution. The effective channel has only a high-conductivity solution, excluding the part of a low-conductivity wall solution (b) Photographs of the main microchannel in which the width of the effective channel (indicated by red lines) varies according to the flow rate of virtual wall solution (0.1, 0.3, 0.4, and 1 μl min^{-1}) with a fixed flow rate of a sample solution (1 μl min^{-1}).

Figure 3-8. Examples of DC impedance signals (ΔZ) of 1.69 μm-sized microparticles according to the various flow rates of virtual wall solution: (a) 0.1, (b) 0.3, (c) 0.5, and (d) 1.0 μl min^{-1}. With a constant size of microparticle, the amplitude of the ΔZ signals varies as a function of the flow rate of the virtual wall solution. Higher flow rate of the virtual wall solution (indicated by nave blue lines) leads to a smaller detection volume. As the detection volume is reduced, ionic flows are perturbed more by the same-sized microparticles, which gives rise to greater amplitudes of the ΔZ signals (red

lines).

Figure 3-9. Representative simultaneous ΔZ and fluorescence signals from 1.69 μm diameter microparticles with different flow rates of virtual wall solution. The tiny ΔZ peaks significantly increase when the flow rate of the virtual wall solution changes from (a) 0.3 to (b) 1 μl min^{-1}, whereas the flow rate of the sample solution remains 1 μl min^{-1}. (c) The peak amplitudes of the ΔZ signals from microparticles (0.99, 1.69, and 4. 16 μm in diameter) increase as the flow rate of the virtual wall solution increases from 0.1 to 1 μl min^{-1} (n = 500).

Figure 3-10. Detection of *F. tularensis*, *E. coli*, and two different types of microparticles. (a) representative DC impedance change (ΔZ) and fluorescence (520 and 610 nm) signals from a sample containing both *F. tularensis* and *E. coli*. The tall ΔZ peaks (green) and the short ΔZ peaks (red) synchronized with the green (520 nm) and the red (610 nm) fluorescence signals, respectively. (b) Distribution profile of the calculated diameters for *F. tularensis*, *E. coli*, and two types of microparticles (n = 500).

Figure 3-11. Distribution profile of the calculated diameters for *F.*

tularensis, *E. coli*, and two different types of microparticles (n = 500).

Table 3-1. The values of the mean (m) and standard deviation (σ) of the ΔZ signal peak amplitudes from various microparticles (0.99, 1.69, and 4.16 μm in diameter) according to the flow rate of the virtual wall solution (0.1, 0.3, 0.5, and 1 μl min^{-1}). ([a]nd = not determined)

Table 3-2. The mean (m) and standard deviation (σ) values of peak amplitudes of the ΔZ signals of the tested samples (*F. tularensis, E. coli*, 0.99 and 1.69 μm in diameter). The flow rates of sample solution and virtual wall solution are fixed at 1 μl min^{-1}.

Table 3-3. The mean (m) and standard deviation (σ) values of calculated diameters of the tested samples (*F. tularensis, E. coli*, 0.99 and 1.69 μm in diameter) from ΔZ peak amplitudes using flow cytometry-based bacterial detection system, assuming a spherical shape of the bacteria. The flow rates of sample solution and virtual wall solution are fixed at 1 μl min^{-1}.

Chapter 1.

Introduction

1. Introduction

1.1. Flow Cytometry

Flow cytometry is a representative technology to analyze multiple parameters of single cells (or particles) based on the analysis results and to count the number of cells, as they flow in a stream of fluid. The measured properties include biophysical characteristics, such as their relative size and granularity, and chemical characteristics such as fluorescence intensity [1].

The first flow cytometry device was Coulter counter in 1950's, which was first disclosed by Wallace H. Coulter [2]. This device was operated based on Coulter principle, which states that particles passing through a small orifice (< 100 ㎛) produces a change in electrical impedance due to the displacement of conductivity between particles and saline solution. The amplitudes and the number of electrical impedance pulses reflect the size and the number of particles flowing through the orifice. Since Coulter counter was a fast and accurate apparatus for particle (or cell) counting and sizing, it is even now widely used in a variety of applications such as biological, chemical and medical areas [3].

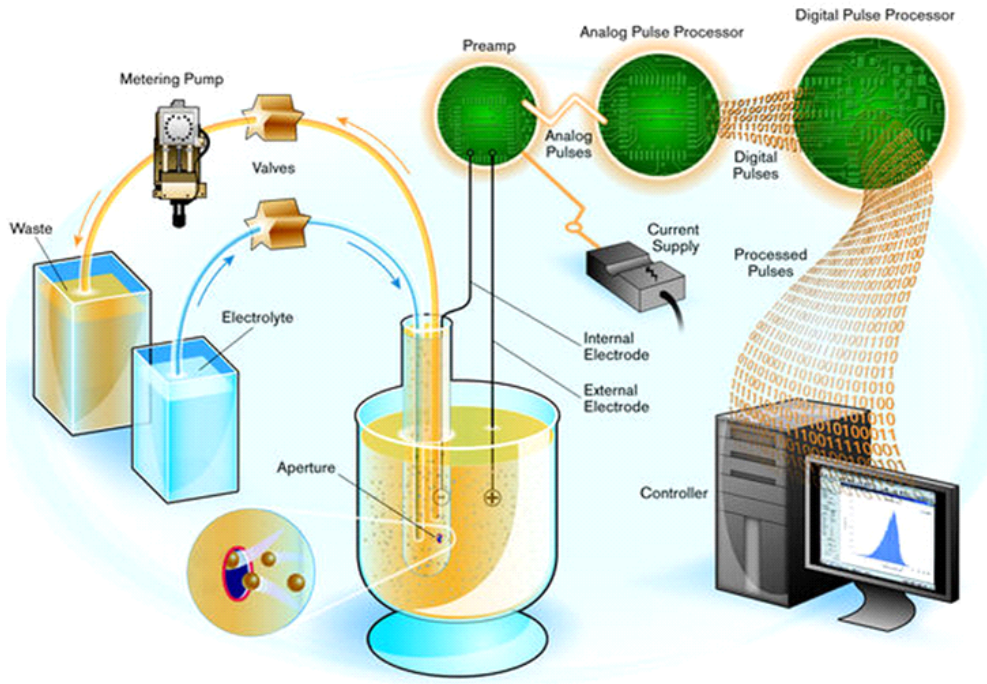

(https://www.beckmancoulter.com/wsrportal/wsrportal.portal?_nfpb=true&_windowLabel=UCM_RENDERER&_urlType=render&wlpUCM_RENDERER_path=%2Fwsr%2Findustrial%2Fparticle-technologies%2Fcoulter-principle%2Findex.htm)

Figure 1-1. Coulter counter diagram with the Coulter principles. A beaker contains microparticles suspended in electrolytic solution and microparticles move through a small aperture on a chamber wall by pump. Two electrodes, one inside and the other one outside an aperture tube, are electrically connected by an ionic flow and measure the impedance change when a particle pass through an aperture. (Beckman Coulter, Inc.)

In the late 1960's, fluorescence measurement had been researched as a mean of analysis in the flow cytometry [4]. Fluorescence measurement could produce both qualitative and quantitative information of particles (or cells). In the same way with coulter counter, fluorescence-based flow cytometry obtains information from suspending particles (or cell) in a fluid stream. When a particle hydrodynamically-focused in the fluid stream is pointed by a laser beams with a s7ingle wavelength, a particle scatters the laser beam in some ways. Scattered lights are divided into forward scattered (FSC) and side scattered (SSC) lights. Among them, the light scattered in the forward direction along the same axis with the laser beam is FSC light and it is correlated with the cell size. The orthogonally scattered light is SSC light and it is proportional to the granularity.

In addition, the fluorescence chemicals in/on the particle are excited and emit the longer wavelength light than the light source. Fluorescent lights are measured by photon detectors such as photomultiplier tub (PMT), photodiode, and charged-coupled device (CCD), with different wavelength bandpass filters, allowing the simultaneous detection of fluorescence at a variety of wavelength from a single cell.

Due to its abilities to analyze multiple information like cytoplasm and cell membrane, fluorescence-based flow cytometry analysis is widely used in researches on cellular activities and clinical applications and diagnosis such as blood analysis.

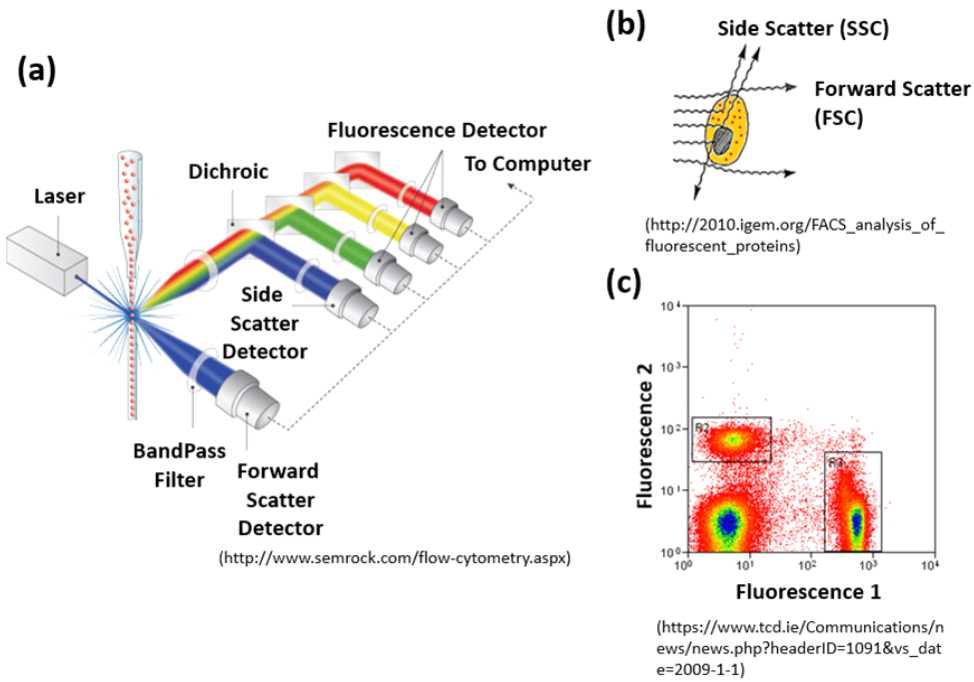

Figure 1-2. Schematic view of optical detection based-flow cytometry. (a) Cells (or particles) flow through the fluid stream and pass by a focused laser beam. By laser beam, fluorescence chemicals on/in a cell get excited and emit the fluorescence. Fluorescence light will be divided into multi-wavelength by various filters and detected by the photon detector such as PMT. (Semrock, Inc.) (b) When a

particle is passing the laser beam, Laser beam will be scattered in some ways; FSC and SSC. (c) The intensity of the fluorescence (or scattered lights) are plotted on graphs.

1.2. Miniaturized Flow Cytometry-based Cell Detection System on a Microfluidic Chip

1.2.1. Microfluidic System

According to the development of microfabrication technology, microfluidic system has been attracted much attention in a multidisciplinary field of biochemistry, nanotechnology, biotechnology, mechanical engineering, and electrical engineering. Microfluidic system is capable of conducting liquid-phase analysis on a microfluidic channel with small volumes of sample fluids and reagents. Due to the microscale, the microfluidic system has unique features compared with the traditional macroscopic system. First of all, the system takes advantages of the benefits of miniaturization: low sample consumption, lower costs, portability, disposability, etc [5]. Secondly, the fluid in the system flows as a laminar flow, allowing multiphase flows because only diffusion on the surface between two solutions is

permitted. Finally, surface-to-volume ratio is significantly high which is enabling reducing reaction time and measurement time, improved sensitivity [6].

With these characteristics, microfluidic technologies led to a lab-on-a-chip (LOC) system which is capable of multi laboratory functions on one small microfluidic chip of a few centimeters in size. Whole processes from beginning to the end for biological or chemical analysis could be performed on a single integrated chip, for example the pre-processing, measurement, and the post-processing.

1.2.2. Importance of Miniaturized Flow Cytometry System

In recent years, flow cytometry has rapidly settled as an indispensable instrument in numerous fields such as molecular biology, pathology, and medicine, ranging from routine blood tests to diagnosis of fatal diseases like leukemia and AIDS (Acquired immune deficiency syndrome) [7, 8]. Despite their significant abilities, standard commercial flow cytometer has a few drawbacks: high costs for maintenance, the size and complexity, being accessible only in major laboratories with specially trained experts. Therefore, the needs for portable, cheap and easy to operate flow cytometry platforms are

increasing, specially in developing countries and first-line clinical offices as well as clinical and biological laboratories. In the future, miniaturized flow cytometry platforms on a microfluidic chip will be utilized as a point-of-care testing (POCT) device for personal disease diagnosis and health monitoring in resource-limited environments and biochemistrical analysis instrument [1].

1.2.3. Approaches for Flow Cytometer-based Cell Detection System on a Microfluidic Chip

Over the past few years, flow cytometry platforms on a microfluidic chip have been researched worldwide [9-11] and rapidly emerging as a promising tool for the clinical usages and biological analyzer at the single-cell level [5, 9, 12].

The most commonly used detection methods for micro flow cytometry are the optical method such as fluorescence and scattered lights detection, and the electrical method such as impedance detection due to the need for the rapid detection of a target cell in the detection region.

A variety of optical detection approaches in micro flow cytometer have been researched. Wolff *et al.* presented a new

pressure-driven microfabricated fluorescent-activated cell sorter (FACS) chip with optical detection components such as 20X objective lens and photomultiplier tube (PMT). With the developed FACS chip, fluorescent latex beads were sorted from red blood cells with a throughput of 12000 cells s^{-1} [13]. Tung *et al.* described poly(dimethylsiloxane) (PDMS)-based micro flow cytometer with two-color, multi-angle fluorescence detection using solid-state lasers and photodiodes. The proposed micro flow cytometer chip was integrated with the microgrooves that make the optical fibers for fluorescence detection and lasers access to microchannels closely [14]. In another study, on a SU-8-based photonic-microfluidic integrated devices, 1, 2, and 5 ㎛ blank beads were measured with 16.4, 11.0, and 12.5 % of coefficient of variation (CV), respectively. In this system, objective lens for light focusing was replaced with on-chip beam shaping and collection structures, enabling system miniaturization [15]. Although various optical detection method-based flow cytometers on a microfluidic chip work successfully with high sensitivity and high-throughput analysis, pre-treatment steps such as cell staining processes are required. Moreover, optical components such as filters, lens, and mirrors cannot be easily miniaturized, disabling system portable.

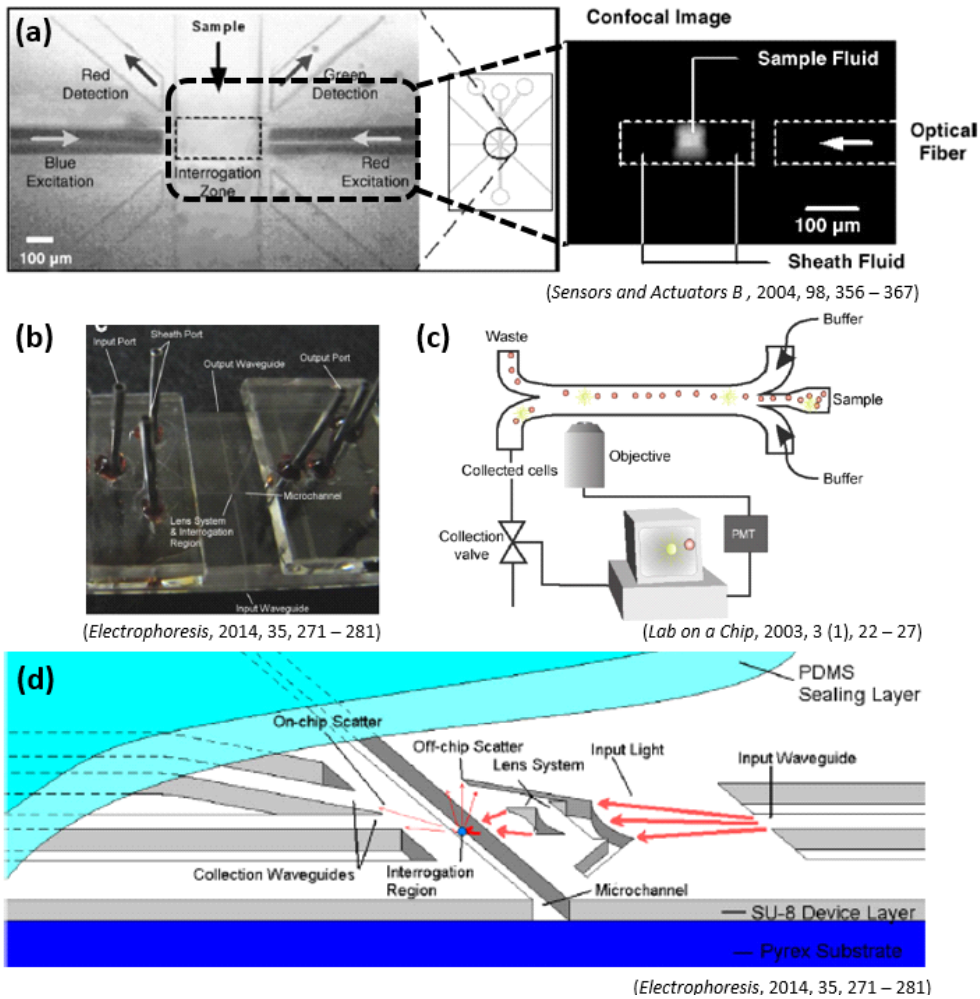

Figure 1-3. Optical detection based-micro flow cytometer system. (a) PDMS-based opto-fluidic micro flow cytometer embedded optical fibers into the microfluidic chip. (b) Packaged microfluidic flow cytometer. (c) Schematic set-up for fluorescence detection-based micro cytometer and cell sorter. (d) Layered structure of the device with the input and output waveguides, lens system, and microchannel

as well as light rays.

On the other hand, electrical detection method-based flow cytometers are able to be operated as a label-free method and does not require a lot of space for components, which is why electrical detection approaches are attractive in terms of simplicity and cost-effectiveness [16]. In addition, impedance detection methods produce more accurate information in terms of cell sizing than scattered light detection methods. Gawad *et al.* suggested a cytometer, based on the micro coulter particle counter (μCPC) principle, for diagnostic applications for cell counting and separation. The device detected individual cells or particles with measuring the impedance at 100 samples s^{-1}. With this device, simultaneous impedance measurements at multiple frequencies were allowed, and detects erythrocytes in buffered solution [17]. Holmes *et al.* developed single cell microfluidic impedance cytometry to identify cells at high speed on the basis of their dielectric properties. Their system used alternating current (AC) impedance detection mechanism to discriminate target cells binded with antibody-conjugated beads. With this system, CD4 T-lymphocytes in human blood were identified and enumerated. They showed that the impedance-based antibody identification method could be the simple low-cost point-of-care

testing (POCT) diagnostic device [18]. Most electrical method-based micro cytometers applied AC voltages due to the electric double layer and faradaic reactions on metal electrodes. In addition, the high frequency AC voltage is more appropriate to eliminate the contact impedance between a metal electrode and the buffer solution. However, because the buffer medium and the cellular cytosol have a similar electrical properties, impedance signal is inversely proportional to the frequency applied. Therefore, recently, researches for the impedance detection method at low frequency have been conducted. Chun *et al.* described DC impedance-based micro cytometer using polyelectrolytic salt bridge-based electrode (PSBE). PSBEs allow to transport ions between the two Ag/AgCl electrodes, decreasing the contact impedance on electrodes. With the developed device with two pairs of PSBEs, red blood cells and white blood cells were detected successfully at 1000 cells s^{-1}. They showed the sensitivity and selectivity in cell detection were remarkably improved than general metal electrode-based micro cytometer [19].

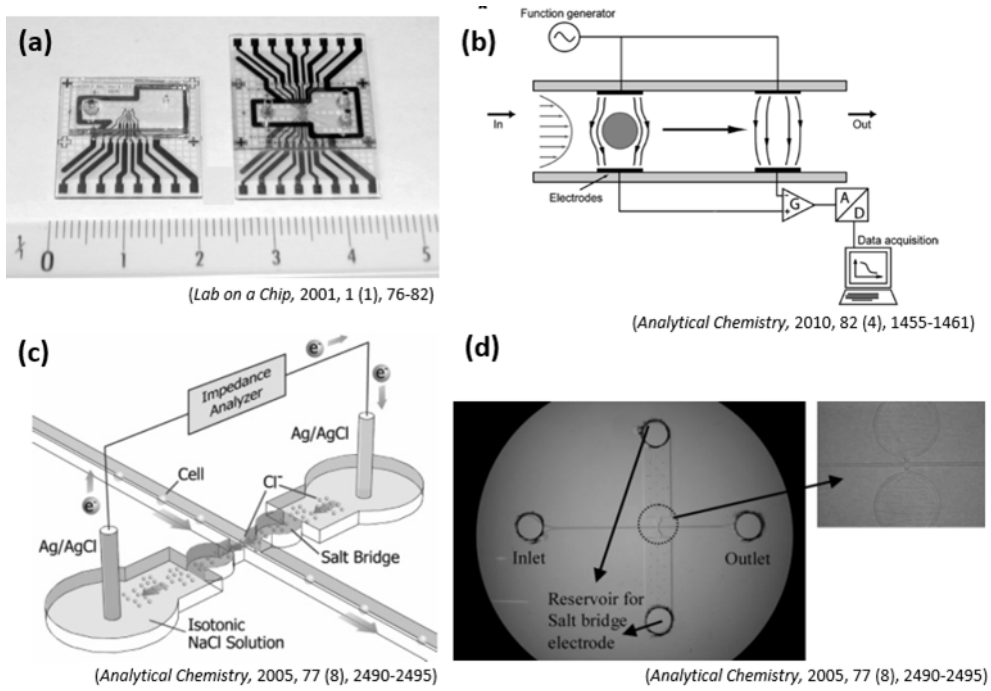

Figure 1-4. Impedance detection-based micro flow cytometer system. (a) The metal electrode patterned microfabricated chip with a PDMS cover and molded fluidic connections. (b) Schematic diagram of the microfluidic AC impedance cytometer using a differential detection. (c) DC impedance analysis with the polyelectrolytic salt bridge-based electrode. (d) Microfluidic glass chip with one pair of polymer.

Nowadays, micro flow cytometry with combination of fluorescence and impedance detection method has been researched to take advantages of both approaches. Barat *et al.* described a microfluidic cytometer that gathered simultaneous optical and electrical properties of particles with measuring SSC light, signal extinction, and fluorescence by PMT and AC impedance at 1 MHz. With the system, a range of different sized polystyrene fluorescent beads were characterized and the results were comparable to the conventional flow cytometer [20]. In another study, a portable microfluidic cytometer with dual detection of DC impedance and fluorescence for cell analysis and particle-based assays was developed. In the proposed system, fluorescence was excited by a light emitting diode (LED) and detected by a solid-stated photomultiplier (SSPM), and DC impedance was measured through polyelectrolyte gel electrodes (PGEs). With dual detection, information of cell existence and size by impedance method, and cellular information by fluorescence method were gathered. With the proposed system, various microbeads and human embryonic kidney 293 (HEK-293) cells were classified [11].

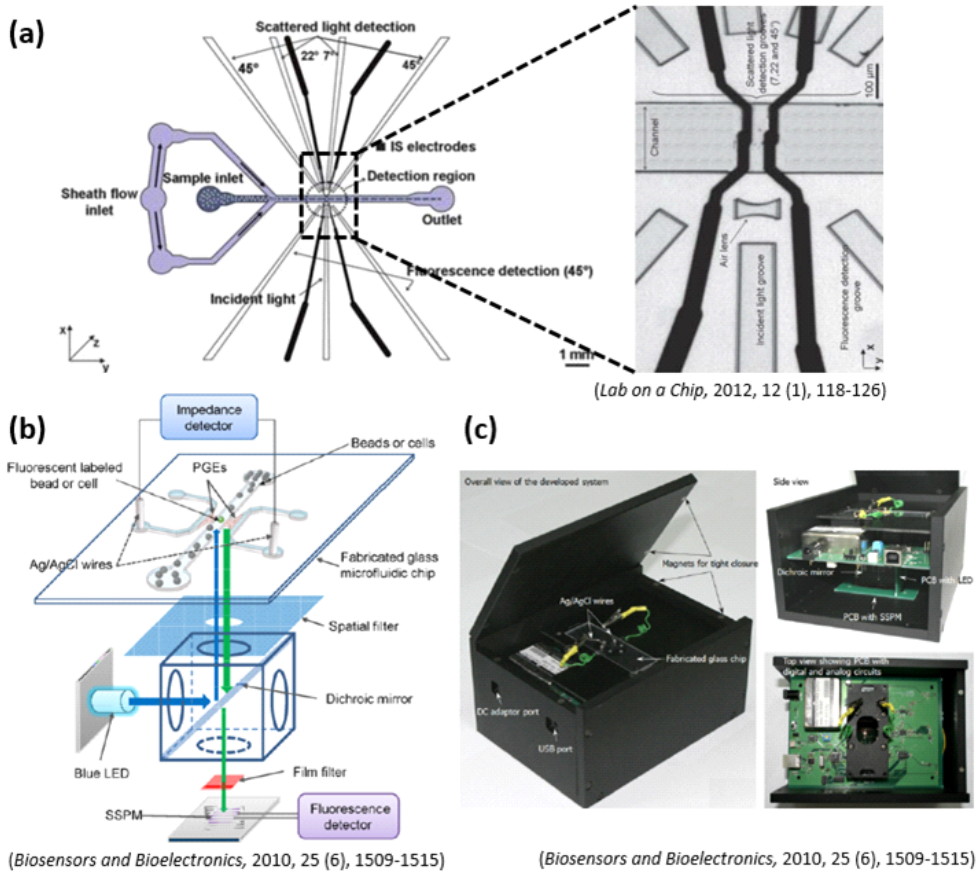

Figure 1-5. Micro flow cytometer system using simultaneous detection of fluorescence and impedance. (a) The cytometer chip with micro-electrodes for impedance spectroscopy (AC impedance) and the different grooves for holding fibers (excitation source and emission paths). (b) Schematic diagram for microfluidic cytometer using DC impedance detection and fluorescence detection with LED and SSPM as a light source and detector, respectively. (c) Pictures of the completed microfluidic cytometer.

1.3. Goals of Study

In the 21st century, with innovative microfabrication techniques and the needs for cellular analysis of a number of biological samples, microfluidics integrated-flow cytometry system have been attracted a great attention due to the simplicity, low-costs, and the high sensitivity with high-throughput. In addition, a portable flow cytometry platform is expected to offer an opportunities of environment screening about air and water examination and daily healthcare by simple blood analysis. Therefore, it is clear that developing flow cytometry platform with microfluidic technology led to personal medical diagnostics and biomedical research worldwide. Hence, many micro flow cytometry platforms have been developed with a variety of detection methods such as optical and electrical methods. Especially, PGE embedded miniaturized flow cytometry platform lowered the contact impedance between electrodes and solution and enabled DC impedance detection for higher sensitivity and better portability. However, there are no many reports or products of microfluidics-integrated portable flow cytometers using a DC impedance detection approach for real life usages. Therefore, the ultimate goal of this study is not only developing a micro flow

cytometry platform using DC impedance and fluorescence detection methods, but also its applications of healthcare and environment screening. In this work, the author presented i) a label-free DC impedance-based microcytometer to count circulating rare cancer cells and ii) flow cytometry-based bacteria detection system using movable virtual wall as a healthcare platform and water examination platform, respectively.

Chapter 2.

A Label-free

DC Impedance-based Microcytometer

for Circulating Rare Cancer Cell Counting

2.1. Introduction

2.1.1. Circulating Tumor Cells (CTCs)

Circulating tumor cells (CTCs), which are disseminated from the primary tumor and circulate in the bloodstream [21], have been attracting much attention in clinical fields, because of the critical roles of CTCs in cancer metastasis. In metastasis processes, CTCs detach from the primary tumor propagate into blood vessels (intravasation), survive in the circulation, attach to a secondary site (extravasation), and grow to form the detectable cancers [22]. In addition, many researches have shown that there is a strong correlation between the number of CTCs and the survival rates of the cancer patients [23-25]. Therefore, simple counting the number of CTCs may serve as a powerful tool for possible cancer diagnosis, prognosis after treatment, and assessment criteria of drug performance [26].

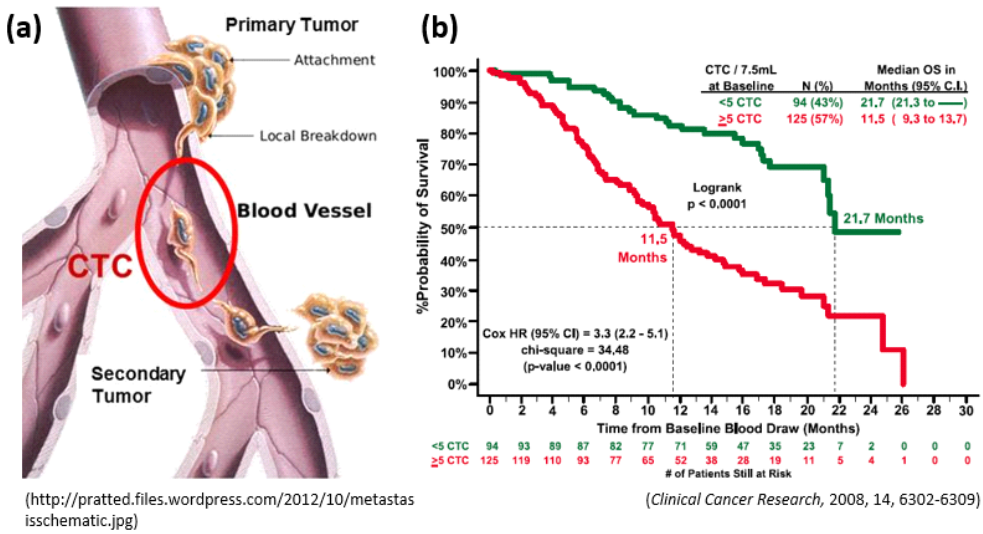

(http://pratted.files.wordpress.com/2012/10/metastasisschematic.jpg)

(*Clinical Cancer Research*, 2008, 14, 6302-6309)

Figure 2-1. (a) From a primary tumor, a subpopulation of cells are detached and propagate into blood circulation. Cells that enter into the blood vessel, which is called circulating tumor cells (CTCs), survive in the circulation and attach to the secondary site, which can grow to secondary tumors. (b) Kaplan-Meier plot shows a relationship between the probability of survival and the time. From the plot, the number of CTCs affect to the survival rates [25].

2.1.2. Approaches for Counting CTCs

2.1.2.1. Conventional Approaches

Epithelial cell adhesion molecule (EpCAM) is a well-known trans-membrane protein expressed on human epithelial carcinomas, such as colorectal, breast, prostate, head and neck, and hepatic carcinomas as well as normal epithelial cells [27-30]. Hence, EpCAM has been one of the best target receptors for antibody-based CTC detection. The CellSearch system (Veridex, NJ) detects CTCs using EpCAM-coated ferrofluids (magnetic nanoparticles), which is currently the only Food and Drug Administration (FDA)-approved device for CTC detection [31]. The FDA-approved CellSearch approach uses EpCAM-coated magnetic bead-based isolation [32-35]. CTC measurements by CellSearch have shown high inter-observer agreement, and they are linear in the range of 5 to more than 1000 CTCs per 7.5 ml of blood [31, 36, 37]. However, it typically identifies CTCs in only half of patients known to have metastatic disease, with an average yield of approximately 1 CTC ml^{-1} and a purity of 0.1 % [31, 38].

CTCs are mostly believed to be larger than peripheral blood

cells, such as red blood cells (RBCs), white blood cells (WBCs), and platelets [39, 40, 41]. Therefore, some approaches use morphological characters of CTCs; the size. ISET (Isolation by Size of Epithelial Tumor cells) device is filtering peripheral blood sample of 1 ml using cylindrical pores with 8 μm diameter, characterizing larger cells left on the filter. [39]. ScreenCell® has a microporous membrane filter and culturing system. Therefore, filtered large cells can be cultured and researched [42].

The classic methods include density gradient separation, which has been implemented using Ficoll-Hypaque (GE Healthcare) or Oncoquick (Greiner Bio-One) to separate CTCs and mononuclear cells from other blood cells [43].

In comparison to the conventional Ficoll procedure, Oncoquick uses a porous membrane to avoid crossover between layers of different cells. Membrane helps keep various fractions from intermixing post-separation, resulting in higher recovery rate [44].
Another classical method is to use magnetic bead-based assays for positive or negative enrichment of CTCs. RosetteSep™ (Stem Cell Technologies), which uses a negative enrichment approach, has demonstrated improved specificity in comparison with standard density gradient procedure. It uses bispecific antibodies that

cross-link unwanted cells in whole blood to erythrocytes, forming immunorosettes, which increases the density of undesired cells allowing their removal by density gradient centrifugation [45, 46]. Though density-gradient cell separation and red blood cell lysis are considered as cell-enrichment methods, these procedures leave CTCs largely outnumbered by peripheral-blood leukocytes.

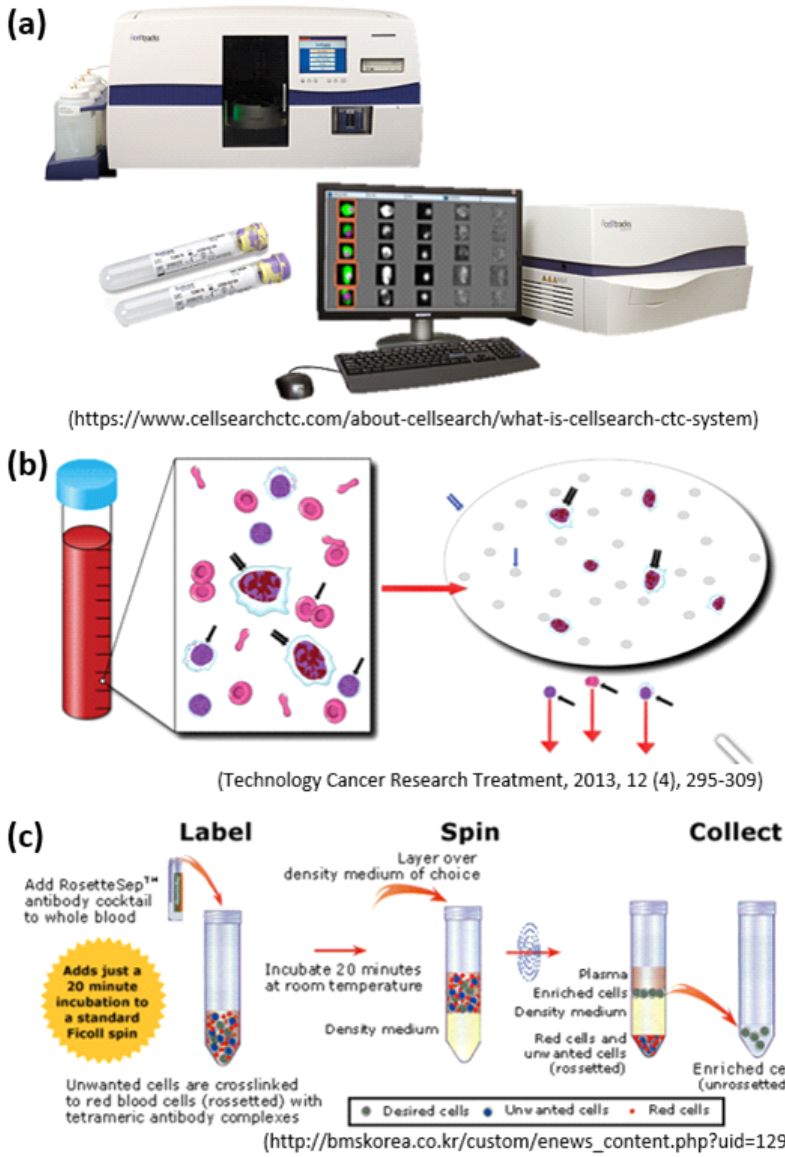

Figure 2-2. Conventional approaches for CTC detection (a) CellSearch system (Veridex, NJ). (b) The principle of ISET (Isolation by Size Epithelial Tumor cells). (c) Process to separate CTCs by RosetteSep™.

2.1.2.2. Microfluidic chip-based Approaches

The most common approaches for CTC detection is affinity binding approaches. Antigen-antibody binding assays are most widely-used for affinity binding assays.

Nagrath *et al.* developed a CTC-chip that had EpCAM-coated microposts on microchannels to capture CTCs, and demonstrated the usefulness of the system using blood samples from the cancer patients [47]. 99 % of isolated CTCs by a CTC-chip were viable and no CTCs was found from healthy subjects. Stott *et al.* described the microvortex generating herringbone chip (HB-chip) for enrichment of prostate cancer CTCs [48]. In comparison to a normal flat-walled microfluidic channel, herringbone-induced microvortices passively mix the blood cells, which disrupt the laminar flow streamlines, increasing surface interaction in the antibody-coated device. At low flow rate of 1.2 ml hr^{-1}, the overall capture efficiencies 29 % ± 4.3 % and 79 % ± 4.5 % in the flat chamber and HB-Chip, respectively reflected the advantage of device structure. Moreover, the HB-Chip yielded 26.3% improved capture efficiency compared with their previous reported CTC-Chip [47]. They also demonstrated its clinical utility in samples from prostate cancer patients and detected CTCs in 14 of 15 patients

with metastatic disease [48].

Recent findings, however, indicate that some invasive tumor cells lose their EpCAM by epithelial-mesenchymal transition (EMT) process [49-51], and some epithelial cells were even found in healthy donors [52]. Furthermore, some leukocytes have been discovered to be positive for EpCAM [53, 54]. For these reasons, EpCAM-based CTC detection often leads to confused results and thus remains a point of controversy [55].

By contrast, morphology-based CTCs detection methods promise high efficiency and cost-effectiveness with label-free approaches [56-59]. Vona et al. found that a significant difference ($P < 0.001$) in cell-area between any carcinoma cell lines and peripheral blood leukocytes [39]. Thus, many research groups have been developing CTC capturing systems based on the size difference of cells.

Filtration is the most common and easiest approach to isolate CTCs based on their size [63, 64]. Some include filtration using the crescent-shaped structures [63] and selective size amplification (SSA) using anti-EpCAM antibody-coated polymer microbeads with multi-obstacle architecture (MOA) filter [64]. In these filtration-based method, however, burst of the cells and mechanical stress-induced

alteration in the original phenotype of the cells can occur as CTCs and peripheral blood cells pass through the pores under high pressure, leading to the loss of the target cells [65, 66].

Hydrodynamic separation techniques use inertial effects that increase in proportion to the cell size to the channel length [67-69]. For one, CTCs were isolated from blood using multi-orifice flow fractionation (MOFF) combined with dielectrophoretic (DEP) cell separation technique [70]. While the hydrodynamic separation method exerts high-throughput with high flow rates, its specificity is extremely low and it needs repeating the whole process for sufficient separation [67-69].

Previously, Soper and colleagues have reported conductivity-based CTC chip, a high throughput microsampling unit (HSMSU) [71, 72]. Interestingly, they could specifically detect CTCs, among other blood cells, employing unique electrical signals from the CTCs passing through the integrated conductivity sensor. However, the conductometric counting requires AC power source that makes the system wired and hardly portable.

2.1.3. Goals of Study

In this chapter, the author present simple, label-free, and efficient DC impedance-based microcytometer for CTC detection. The microcytometer detects DC impedance change corresponding to the volume of a cell between polyelectrolyte gel electrodes (PGEs). Previously, our group proposed a microcytometer system using PGEs to count microbeads, RBCs, and WBCs [11, 19, 73]. The whole system, however, had to be redesigned to tolerate intense flow of larger quantity of blood samples that contains CTCs without compromising the impedance measurement. First, the author used double sheath flow to decrease cell adhesion to inlet and channel walls while increasing the sensitivity. Second, the author have thickened the PGEs to withstand high pressure under high flow rates. Third, the author optimized the DC impedance detection system to comply with the demand of the newly designed chip. Here, the author show that the proposed system can not only detect ovarian cancer cells spiked in blood samples, but also be used for the diagnosis of cancer patients. The impedance microcytometer obviates labeling, and dilution process while holding a high efficiency of ~88 % and a flow rate of ~13 μl min^{-1}.

2.2. System Scheme

Figure 2-3 shows a schematic diagram of the DC impedance-based microcytometer for CTC detection. The system comprises of a PGE-integrated microfluidic chip, an impedance detection circuit, and a signal acquisition system. The microfluidic chip consists of microchannels for sample loading, sheath flow generation and two big reservoirs for PGEs and ionic solution like PBS or 1 M KCl (Figure 2-3(a)). The PGE detection region of microfluidic chip is 70 μm wide and 25 μm high. A sample, once introduced through sample inlet, is hydrodynamically focused twice by sheath fluid of phosphate buffered saline (PBS, pH 7.4) solution (2-D hydrodynamic focusing). The sheath flow prevents cell adhesion to chambers and channels, reducing sample loss. Since the PGEs have the same height with the channel walls, the impedance signals are not affected by the *z*-directional positions of a passing particle.

The customized impedance detection circuit is designed with a custom printed circuit board (PCB) implemented with rectifiers, amplifiers, and filters to remove noises and to amplify only necessary signals. Acquired signal is displayed and stored by custom software using LabView software (National Instrument). Figure 2-3(d) shows a photograph of a microfluidic chip of which length is 39 mm.

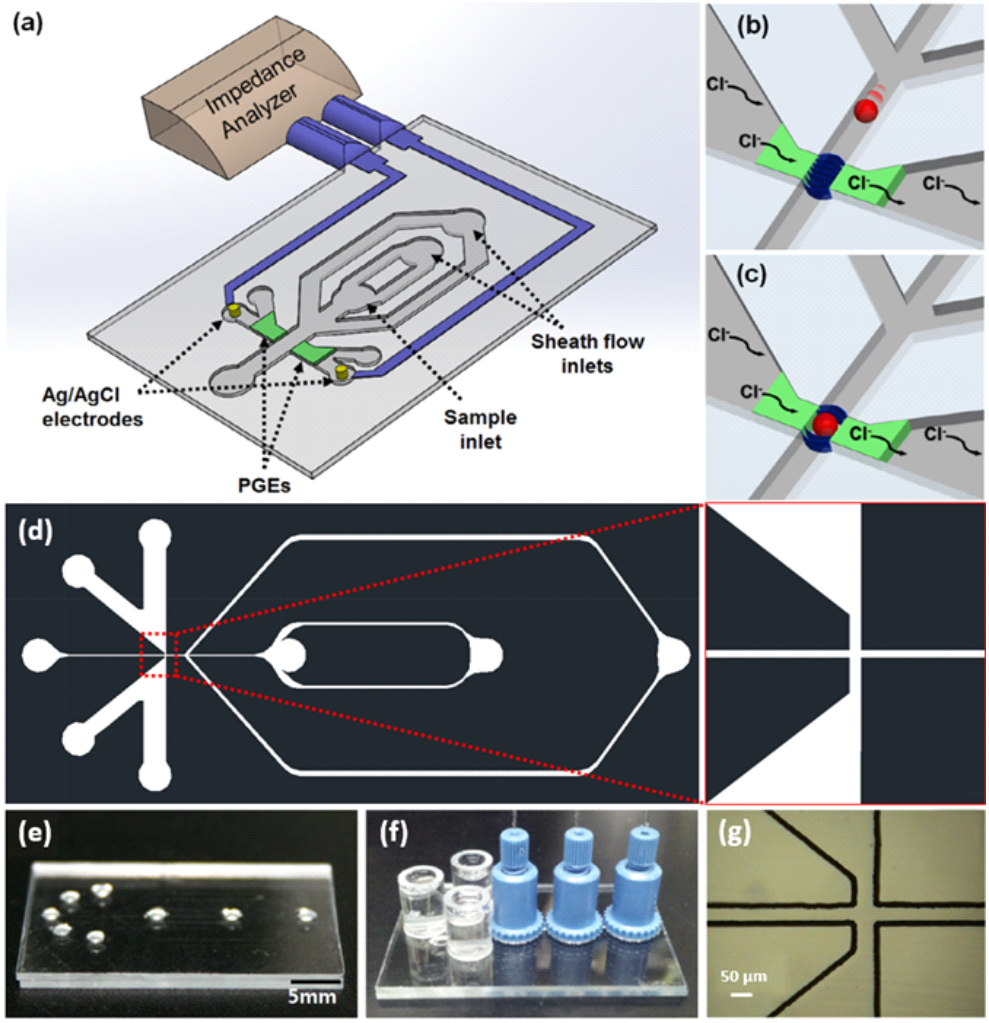

Figure 2-3. (a) Schematic illustration of the DC impedance-based cell counter. Ionic flows between the PGEs under low DC bias (b) are interrupted when a cell passes through, causing a DC impedance change (c). (d) Film mask image for the microfluidic chip and the enlarged image of detection region. A photograph of the microfluidic glass chip (e) equipped with a fluidic connection with NanoPort

Assemblies (Upchurch) (f). (g) Enlarged image of the detection region in the fabricated microfluidic glass chip. The main channel is 70 μm wide and 25 μm high.

2.3. Experimental Method

2.3.1. Sample Preparation

To evaluate the performance of the system, we used fluorescent microbeads (Bangs Laboratory). The average diameters of the beads are 8.31 and 10.35 μm similar to the peripheral blood cells, and 15.02 μm, comparable to the CTCs. The beads were suspended in 1 M KCl before use.

Normal blood samples were collected in EDTA treated Vacutainer tubes (BD, NJ) from healthy volunteers. To elucidate the information about the size distribution of WBCs, normal blood samples were diluted at a ratio of 1:10000, and labelled with CD45 antibody from (Abcam) and then secondary antibodies conjugated with Alexa 610PE (Invitrogen). The OVCAR-3 cancer cell lines were grown in 100 mm culture dish (SPL Life sciences) with RPMI 1640 containing 10 % (v/v) fetal bovine serum (FBS) and 1 % penicillin and streptomycin (P/S)

(WelGENS Inc.) at 37°C/5 % $CO^{2.}$ The cells were detached with 0.05 % trypsin-EDTA (WelGENS Inc.) and diluted at a ratio of 1:5 every three days.

For the verification of impedance threshold for CTC counting, the OVCAR-3 cells were stained with EpCAM antibody (Santa Cruz Biotechnology) and secondary antibody conjugated with FITC (Invitrogen), followed by simultaneous measurement of fluorescence and impedance. To generate a calibration curve, the cells were counted by a hemacytometer and diluted with PBS (pH 7.4) to reconstitute 10, 100, 500, and 1,000 cells per 10 μl of PBS. Then, the cells with known numbers were spiked in 500 μl of normal blood.

The blood samples from 24 patients with metastatic breast cancer (stage IV, median age 52) were obtained from National Cancer Center (NCC) of Korea (Institutional Review Board number NCCNCS-12-624). For the confirmation of the impedance peaks, patient blood samples were labelled with Her2 antibody (Abcam) and secondary antibodies conjugated with Alexa 610PE (Invitrogen). All blood samples were centrifuged and the blood plasma was replaced with the same amount of PBS (pH 7.4) containing 3 % albumin to prevent adsorption of cells to the channel walls.

2.3.2. Experimental Setup

For the impedance signal calibration based on size, fluorescent microbeads with different sizes (8.31, 10.35, and 15.02 μm diameter) in 500 μl PBS were injected into the sample inlet at a flow rate of 13 μl min^{-1}. To generate sheath flow, 1 M KCl solution was introduced into the first and second reservoir at a flow rate of 13 and 41 μl min^{-1}, respectively by a syringe pump (KDS 200, KD Scientific Inc.). For the test of blood samples, 500 μl of spiked or clinical blood samples were injected into the sample inlet at a flow rate of 13 μl min^{-1}. The interfaces between syringe pumps and the microfluidic chip were connected by 100 μm diameter capillaries (Polymicro Technologies) with Nano Port Assemblies (Upchurch) (Figure 2-3(e)). The capillaries were cleaned with PBS/albumin solution to prevent cell adhesion to the capillary walls.

Custom-made impedance detection circuit generated 0.4 V DC bias between the two Ag/AgCl electrodes and detected the impedance change between PGEs. The data signal was transmitted through the DAQ card (National Instrument) at 10 kHz sampling rates. Acquired signal was processed with software filters to compensate a base line drift, displayed and saved by self-programmed LabView software.

For the simultaneous detection of fluorescence and DC impedance, Ar laser (488 nm) was focused on the detection region in between PGEs by objective lens (40×, Nikon). The fluorescence signal, filtered by 510/42 and 610/54 band-pass filter (Thorlabs), is detected by photomultiplier tube (PMT) (Hamamatsu), while the impedance change was detected by DC impedance detection system.

2.4. Results & Discussion

2.4.1. System Calibration

As shown in Figure 2-3(b) and (c), PGEs not only separate main microchannel from Ag/AgCl electrode chambers physically, but also transport ions between the two Ag/AgCl electrodes. By applying a constant DC voltage to the Ag/AgCl electrodes, ions transport to the opposite pole through the PGEs. Because the cell membrane behaves like an insulator and the DC cannot flow through the cell body, the ionic flows are hindered by the presence of a cell between the PGEs. Thus, unlike AC impedance methods, the DC impedance peaks contain accurate information about the cell volume, yielding the same peak amplitude for the same particle size [70, 74].

The resistance change of ionic current (ΔR) between the PGEs is defined by the resistivity of electrolyte and the volume fraction of a particle to a detection area:

$$\triangle R = \frac{4\rho_m d_p^3}{\pi D_t^4}$$

where D_t is the cross-sectional-area of a detection region, d_p is the diameter of a particle or a cell, and ρ_m is the resistivity of electrolyte [74]. Because every factor, except particle diameter, is constant, the change of resistivity is proportional to the cubic diameter that is the volume of a particle. Indeed, when we compared the peak amplitude of impedance signal to the volume of the various microbeads, we obtained a good linearity with R^2 = 0.9949 (Figure 2-4(a)). Thus, even a small change in diameter can lead to sufficiently large difference in resistance to be detected.

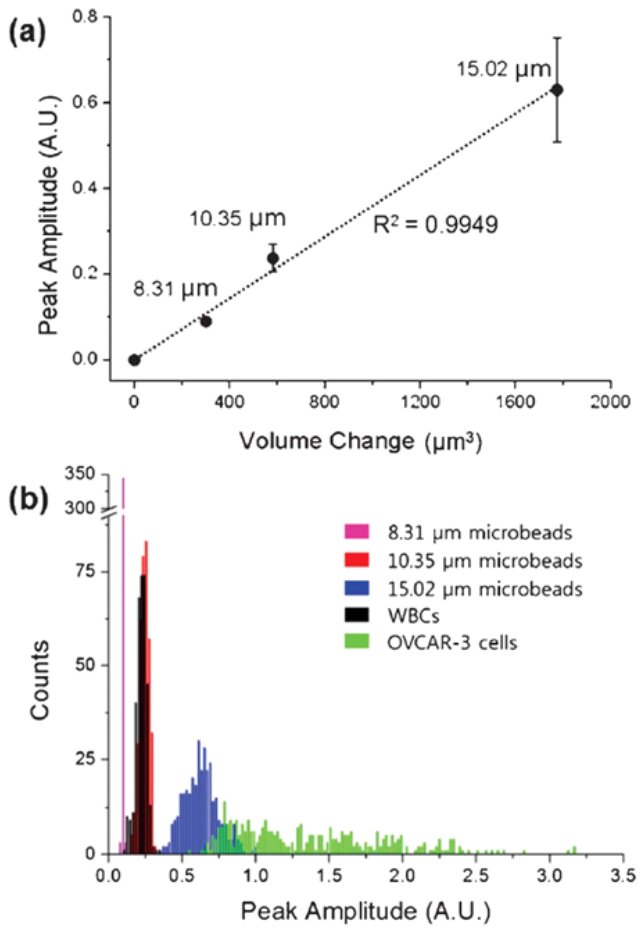

Figure 2-4. (a) Calibration curve of the impedance peak amplitude corresponding to the volumes of 8.31, 10.35, and 15.02 μm diameter particles. Standard error bars are from five independent experiments. (b) Histogram of the impedance peak amplitude obtained from various microbeads, WBCs, and ovarian cancer cell lines (OVCAR-3). The WBCs were fluorescently labelled using a CD45 antibody, and the impedance peaks that synchronize with fluorescent peaks were counted.

Table 2-1. The mean (m) and standard deviation (σ) values of impedance peak amplitudes for the various microbeads, WBCs and OVCAR-3 cells.

Targets	Mean (m)	SD (σ)
8.31 μm	0.090	0.003
10.35 μm	0.237	0.032
15.03 μm	0.630	0.121
WBCs	0.227	0.034
OVCAR-3 cells	1.372	0.526

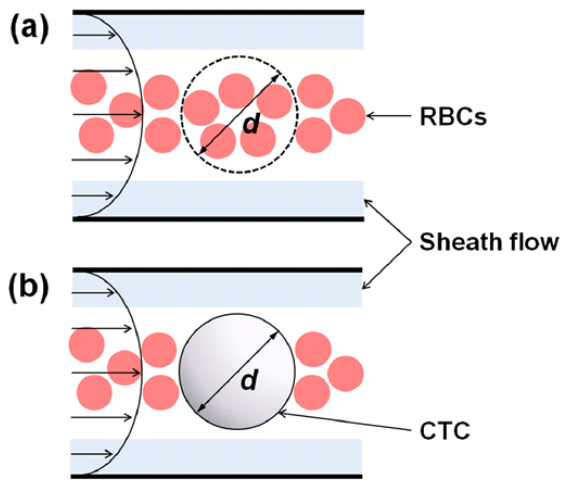

Figure 2-5. Schematics for normal blood cells (a) and a cancer cell (b) in blood samples flowing through microchannels. In (a), RBCs occupy about 45 % of the volume of one CTC with a diameter of d. Other minor blood cells are ignored.

2.4.2. Size Distribution of Ovarian Cancer Cells

The author chose ovarian cancer cell lines (OVCAR-3) as a model system for CTCs. We analyzed the size distribution of OVCAR-3 cells suspended in PBS (pH 7.4) on the basis of the calibration data (see Figure 2-3). Figure 2-4(b) displays a histogram of peak amplitude for comparing OVCAR-3 cells with WBCs and various microbeads of different diameters. The statistics, including mean (m) and standard deviation (σ) values of the peak amplitudes, for three types of microbeads, WBCs and OVCAR-3 cells are listed in Table 2-1.

Despite the frequent concerns about size overlapping between large leukocytes and CTCs, we observed no such overlapping between WBCs and OVCAR-3 cells (Figure 2-4(b)). The size of WBCs measured in our system was much lower than expected, ranging 7.3~11.2 μm, while the ones of OVCAR-3 cells were translated into cell sizes ranging 16~25 μm in diameter. Indeed, Lara et al. reported that the diameters of most blood cells were not larger than 13 μm [40], which was recently confirmed by Holmes et al. who reported that the size of white blood cells vary from 6 to 12 μm [75]. Thus, the OVCAR-3 cells, and other cancer cells with similar or

even smaller sizes, are clearly distinguishable from blood cells including RBCs, WBCs, and platelets. However, in general, we cannot rule out the possibility that rare population of large leukocytes can participate in CTC enumeration when using patient blood by simple impedance-based counting. As such, if required, we conducted simultaneous detection of fluorescence and impedance signals to verify the impedance peaks from patient blood samples (vide infra).

2.4.3. Counting Efficiency of Rare Cells in Blood

Normally, hematocrit, a volume percentage (%) of RBCs in blood, is ~45 % [76]. Thus, if the volume of an OVCAR-3 cell is replaced by blood, the RBCs will take ~45 % of the volume of the OVCAR-3 cell. That being said, the unoccupied volume, in this case ~55 % of the cell volume, is responsible for the resistance change when an OVCAR-3 cell, instead of blood, passes through the detection region (Figure 2-5). When a cell with 16 μm in diameter replaces blood, the volume change is given as

$$\triangle V = \frac{4}{3}\pi(\frac{1}{2}d)^3 \times (1-0.45) \approx 1180\mu m^3$$

that corresponds to the volume of ~13.1 μm diameter sphere of which impedance peak amplitude is 0.4 (see Figure 2-4). Therefore, we set 0.4 as the threshold for the detection of OVCAR-3 cells with the minimum diameter of 16 μm.

To identify the peaks from the cancer cells in blood samples, we compared two kinds of samples with simultaneous detection of fluorescence and DC impedance: normal blood and blood samples spiked with OVCAR-3 cells stained with FITC-conjugated EpCAM antibody. Normal blood samples, containing various blood cells, yield

thick baseline with amplitude of ~0.03. Several taller peaks, probably due to the large leukocytes, were also observed below the threshold, which failed to generate fluorescence peaks (Figure 2-6(a)). On the contrary, the blood sample spiked with OVCAR-3 cells produced impedance peaks over the threshold (Figure 2-6(b)), all of which were synchronized with fluorescence events. Therefore, we successfully confirmed that the impedance peaks over the threshold indicate the existence of cancer cells.

To determine the counting efficiency, we spiked 10, 50, 100 and 1,000 cancer cells in 500 μl of blood obtained from healthy donors. The counting efficiency reaches 88 % and linear over the entire range tested (Figure 2-6(c)). Of note, we could observe the linearity of the counting efficiency over the range tested with R^2 = 0.9999. Taken together, these performances satisfy the conditions to be a successful system for rare cell detection.

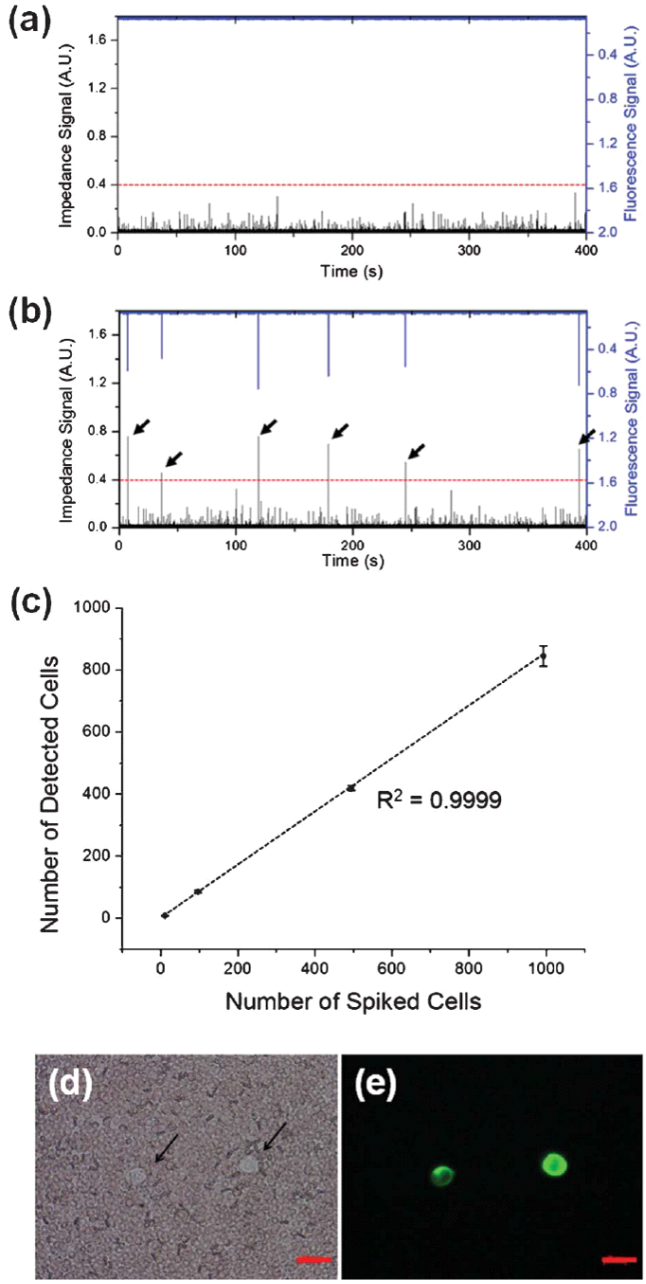

Figure 2-6. Simultaneous impedance and fluorescence signals from normal blood samples of healthy volunteers (a), and from OVCAR-3

cells spiked into normal blood (b) after labeling with EpCAM antibody. In (b), the peaks over the impedance threshold (0.4) synchronize with fluorescence peaks. (c) The counting efficiency is about 88 % and is linear over the entire range under the optimal flow rate (R2 = 0.999) when a range of cells (10, 100, 500, and 1000 cells) was spiked in healthy normal blood samples. Standard error bars are from five independent experiments. Light (d) and fluorescence (e) images of EpCAM-labeled OVCAR-3 cancer cells spiked into blood. Scale bar = 20 μm.

2.4.4. Patient Sample Test

The author then tested the applicability of the DC impedance-based microcytometer for cancer diagnosis using blood samples from cancer patients (Figure 2-7). Breast cancer cells (MCF-7) are one of the smallest cancer cells with the diameter of 17~28 μm [39], which is comparable to the measured size of model OVCAR-3 cancer cells that range 16~25 μm in diameter (see Figure 2-4) Therefore, we reasoned that the impedance threshold for OVCAR-3 cells could be conservatively applied to the enumeration of breast cancer cells.

To verify that the impedance peaks over the threshold originate from cancer cells, we stained patient blood samples with Alexa 610PE-conjugated Her2 antibody, and detected fluorescence and impedance signals simultaneously. As shown in Figure 2-7(a), all the impedance peaks over the threshold (black arrows) synchronized with fluorescence peaks. Note that there are Her2 positive peaks that fall short of impedance threshold (within broken lines), possibly indicating small-sized CTCs. There are also impedance peaks almost touching the threshold bar with no fluorescence signals. These results show that the Her2 fluorescence signals were cancer-specific and not from

size-based background. When we labelled patient blood with CD45 antibody, no significant fluorescence signal was found for the impedance peaks over the threshold.

In all 24 blood samples from cancer patients, our system detected tall peaks satisfying the 0.4 impedance criterion (see Figure 2-7(b)). The number of effective peaks varied from 1 to 20, whereas no such peaks were detected from blood samples of five healthy volunteers. We also analyzed three blood samples from patients who have finished chemotherapy treatment. Indeed, two out of three samples yielded no such peaks over the impedance threshold (Figure 2-7(b)).

The results clearly demonstrate that the proposed cytometer is capable of distinguishing DC impedance peaks between normal and patient blood samples.

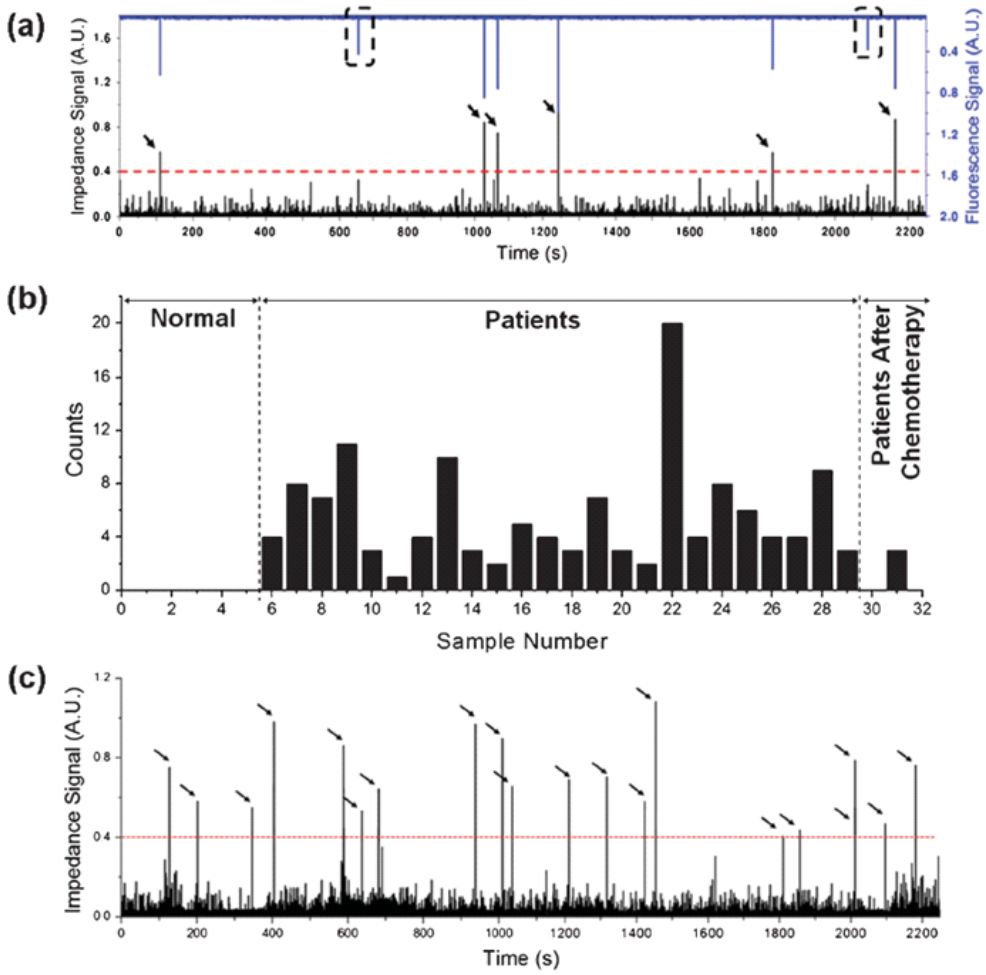

Figure 2-7. Detection of CTCs from blood samples (500 μl) of breast cancer patients in stage Ⅳ. (a) Simultaneous measurement of fluorescence and impedance signals from patient blood stained with Her2 antibody. The peaks in broken lines indicate cells with Her2 positive but below the impedance threshold. (b) Impedance peaks over the threshold value were detected and counted in all of the 24 blood

samples from patients, whereas no such peaks were detected in blood samples from 5 healthy donors. In two out of three blood samples from patients who have finished chemotherapy treatment, no impedance peaks over the impedance threshold were detected. (c) Representative impedance signals from the 22^{nd} patient sample.

2.5. Conclusion and Perspective

In this chapter, the author demonstrated a label-free DC impedance-based microcytometer system for efficient counting of circulating rare cancer cells in blood without labeling and dilution. We successfully measured impedance changes in between PGEs caused by non-conducting large cells in blood. Using this method, after verification of volume-impedance linearity, the author obtained 88 % detection efficiency for OVCAR-3 cells spiked in 500 μl of blood. In addition, we obtained positive results from all of the blood samples from breast cancer patients in stage IV, whereas largely negative results from patients who finished chemotherapy treatment, indicating that the proposed microcytometer has a potential to distinguish cancer patients from healthy normal people and to provide information about the current state of cancer.

However, still understanding of CTCs' biological properties and clinical roles has been limited due to the lack of availability of technologies to isolate CTCs with a sufficient purity and conditions which enable to study their molecular and functional experiments [77]. Nowadays, therefore, there have been the developments of advanced and sensitive technologies to capture human CTCs to

provide the opportunity to extend studies of relationship between the number of CTCs and cancer metastasis [78, 79]. The author hope that in the near future, their relation is proved with the scientific evidences clearly and the developed DC impedance-based micro CTC cytometer will be utilized for a facile and fast way of cancer diagnosis at the site of patient care, which will help with prompt decisions for further in-depth investigation of the disease.

2.6. Further Study

The developed DC impedance-based micro CTC counter utilizes 500 μl of blood for one test for approximately 40 minutes. However, the only FDA-approved CTC detection system, The CellSearch system, examines 7.5 ml of blood sample for one test, which means that the test results from 7.5 ml of blood only can be accepted officially and 500 μl of blood could be insufficient for cancer diagnosis for early stage cancer patients. Therefore, the proposed DC impedance-based microcytometer requires further study for handling large volume within limited time. The simplicity of the microchannel design and the electrical circuits opens up the possibility of easy parallelization for the simultaneous analysis of large volumes of blood

in a short time. (Refer to the appendix section c for further study plans.)

Publications

Hyoungseon Choi, Kwang Bok Kim, Chang Su Jeon, Inseong Hwang, Saram Lee, Hark Kyun Kim, Hee Chan Kim and Taek Dong Chung, "A Label-free DC Impedance-based Microcytometer for Circulating Rare Cancer Cell Counting", ***Lab on a Chip***, 2013, 13(5), 970-977.

Chapter 3.

Flow Cytometry-based Submicron-sized Bacteria Detection System using Movable Virtual Wall

3.1. Introduction

3.1.1. Importance of Bacteria Detection

Bacteria and microorganisms are extremely diverse and widespread in nature. There are more than 10^{30} kinds of bacteria in the world [80]. Although most bacteria are harmless and sometimes even advantageous to plants and animals, some are severely pathogenic. Infectious diseases caused by food- and waterborne pathogens, such as *Salmonella sp.*, *Escherichia coli*, *Campylobacter coli*, and *Bacillus cereus*, cause 25 % of the fifty millions of estimated deaths worldwide, and 45 % of deaths in low-income countries [81-84]. Among others, *Bacillus anthracis*, *Francisella tularensis*, and *Yersinia pestis* are considered as biological warfare agents that cause lethal symptoms with a low infectious dose, necessitating the development of devices for fast, sensitive, and accurate detection [85, 86].

3.1.2. Approaches for Bacteria Detection

Conventionally, bacterial detection has been conducted by

liquid culture or colony counting, which is labor-intensive and time-consuming. To overcome those limitations, PCR-based, label-free, immunoreaction-based, and flow cytometry-based bacterial detection systems have been developed. However, PCR-based sensors require long process times and relatively pure samples, whereas most biological samples are complex [87, 88]. Although label-free methods can secure fast detection by measuring electrical or optical changes in biochemical [89, 90] and physical [91] properties of bacterial environments, application of these is limited owing to a lack of sensitivity as well as selectivity.

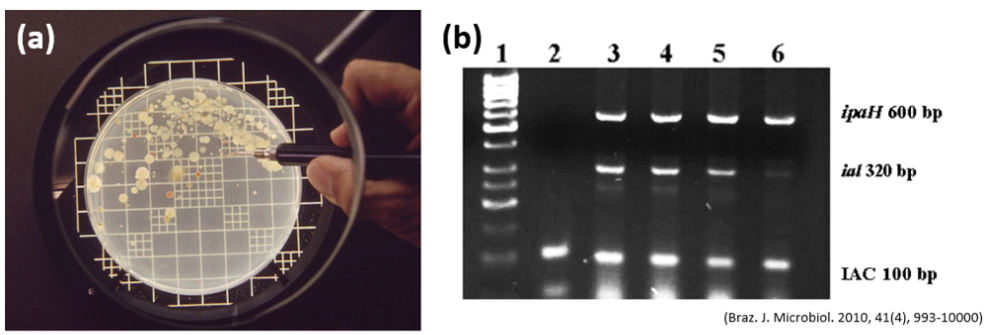

Figure 3-1. Conventional approaches for bacteria detection system. (a) Colony counting method. (b) Polymerase chain reaction (PCR)-based method.

Immunoreaction, probably one of the most frequently used methods, has been applied to detect *Bacillus globigii* and *E. coli* by employing a complementary metal oxide semiconductor (CMOS) immunosensor [92] and magneto- immunosensor [93], respectively. In general, immunoreaction-based sensors still need to be improved in terms of throughput and turnaround time.

In this context, flow cytometry-based approaches are attracting attention because of the capability to detect individual bacteria, ensuring both qualitative and quantitative specificities [94, 95] and providing multiplexed information [96]. Recently, Kim et al (2013) presented a microfluidic multichannel cytometer using a three planar electrode potentiometric system [97] The cytometer could discriminate between microbeads (diameters ranging from 2-3.5 μm) and *Bacillus subtilis* (diameter, ~1 μm; length, ~4 μm). However, limitation of the channel dimension prevented analysis of submicron particles. For higher sensitivity, a microfluidic AC (alternating current) impedance cytometer was developed, in which the channel width was reduced by two-dimensional (2-D) hydrodynamic focusing to detect micron-sized particles and bacteria [98]. However, the AC-driven apparatus is not the best choice for point-of-care devices due to its portability and complexity. For the detection of

submicron-sized particles such as viruses and synthetic nanoparticles, a specific device harnessing resistive pulses from nanopores was proposed [99]. As such, there remain challenges as well as opportunities in providing cytometric sensors with tolerance for wide ranges of particle size, as well as portability for onsite detection of pathogenic microbes whose size distributions are distinct from each other.

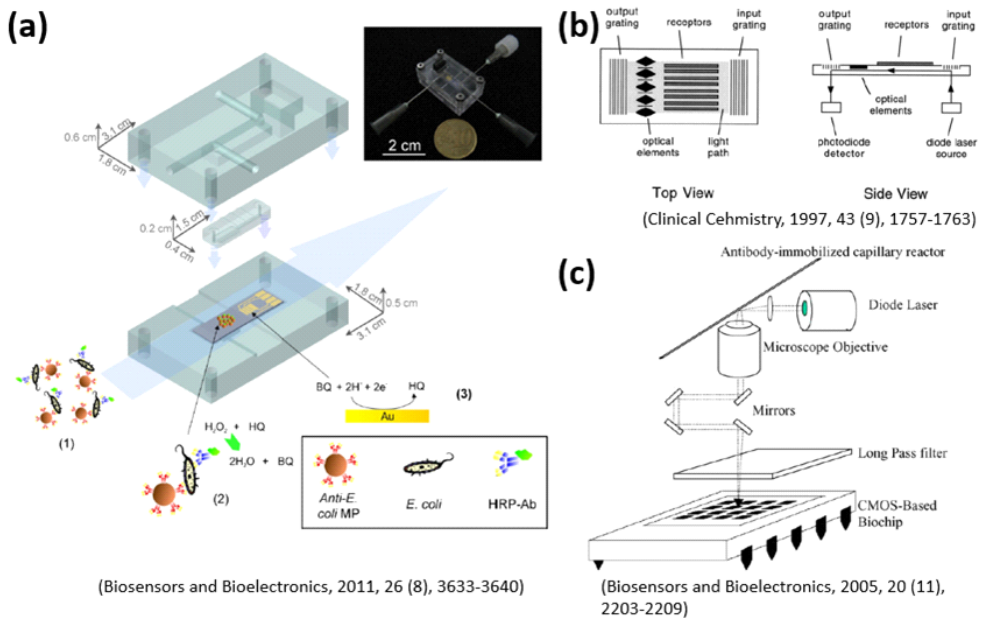

Figure 3-2. Various bacteria detection system. (a) Scheme of the microfluidic system, which consists of microchannel for bacteria immunocaptured with magnetic particles, and gold electrodes for reduction of enzyme-produced *p*-benzoquinone (BQ). (b) Schematic view of the Hartman interferometer. A single planar wave of linearly polarized light is coupled into a thin waveguiding layer. (c) CMOS biochip immunosensor for detection of a single bacteria.

3.1.3. Goals of Study

In this report, the author suggest a miniaturized flow cytometry-based bacterial detection system equipped with a movable virtual wall. The flexibility of the channel dimension enables detection of particles with various sizes ranging from submicron to several micron dimensions. The simultaneous detection of DC impedance and fluorescence signals ensures selectivity and sensitivity to specific targets. Previously, we proposed a portable flow cytometer that can count microbeads, blood cells, and CTCs [11, 19, 100], which is not appropriate for detection of cells smaller than 5 μm in diameter owing to the geometric limitations of microchannels. Here, by virtue of a movable virtual wall made of a non-conducting solution and new chip design, we show that even submicron-sized *F. tularensis* could be successfully counted. The author also demonstrate that the proposed device can discriminate between *F. tularensis* and *E. coli* BL21 that have different gamuts of size distributions.

3.2. System Scheme

The flow cytometry-based bacterial detection system is

comprised of a PGE-integrated microfluidic chip, DC impedance change (ΔZ) detection circuit, fluorescence detection system, and signal acquisition system. The microfluidic chip has microchannels for samples (high-conductivity), a virtual wall solution (low-conductivity), and two large reservoirs that contain Ag/AgCl electrodes, PGEs, and ionic solutions (PBS or 1M KCl) (Figure 3-2(a)). The detection region between the two PGEs measures 140 μm long and 7 μm high. The samples loaded through the inlet were hydrodynamically pushed toward the PGEs wall by the virtual wall solution. The extremely low ion conductivity of the virtual wall solution makes it behave like an insulating wall. The channel width of the detection region was adjusted by the flow rate of the virtual wall solution (see Figure 3-3). When the flow rate of the virtual wall solution is low, the microfluidic channel allows a wide detection area. The wide channel is suitable for the detection of several micron-sized particles; it is inappropriate for detection of submicron particles owing to the relatively low density of ionic current within the detection region (Figure 3-2(b)). In contrast, higher flow rate of the wall solution narrows the effective channel width, which leads to a smaller detection region and thus higher sensitivity (Figure. 3-2(c)). Consequently, submicron particles generate significant impedance

signals that are otherwise impossible to detect. Fluorescence was simultaneously monitored in between the two PGEs so that the fluorescence signals lie in the middle of the two impedance signals (Figure 3-2(b) and (c)).

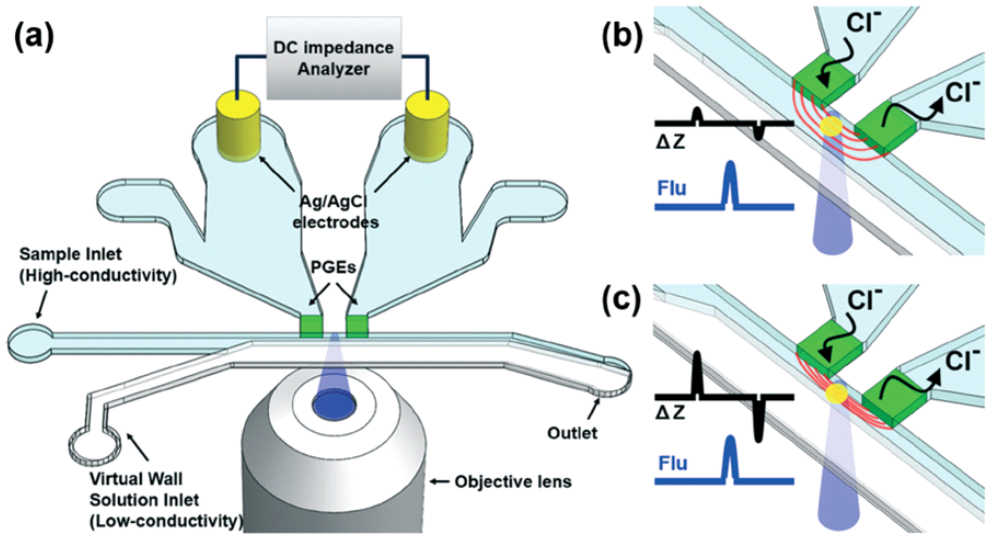

Figure 3-3. (a) Schematic illustration of the flow cytometry-based submicron-sized bacterial detection system. (b) A virtual wall solution with a slow flow rate, although enabling detection of large particles, renders a relatively low current density and a wide channel width, preventing detection of submicron particles. (c) Fast flow of the wall solution narrows the channel, yielding higher current density and thus greater DC impedance change (ΔZ) required for detection of submicron particles (figures not drawn to scale).

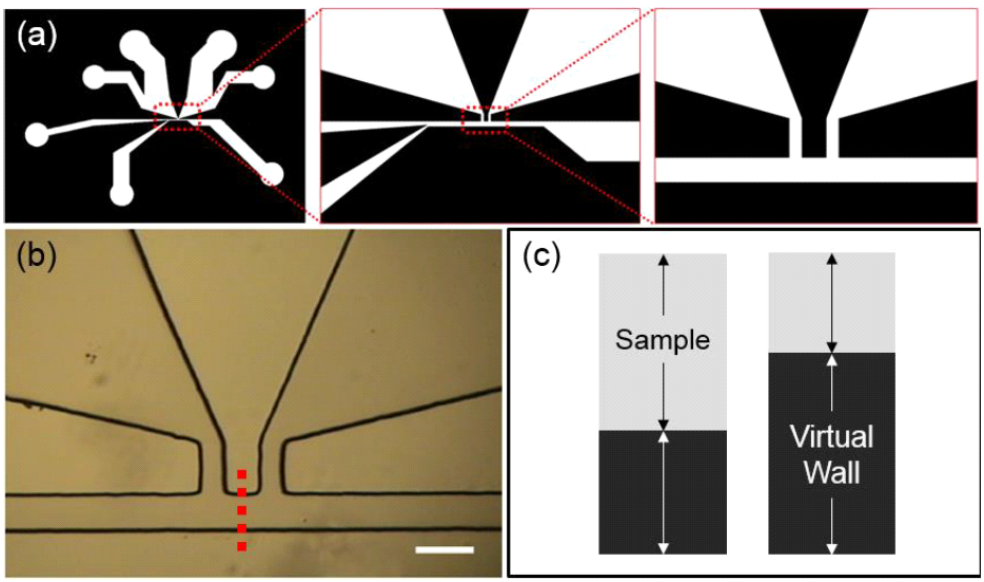

Figure 3-4. (a) Mask pattern of the microfluidic chip for the flow cytometry-based submicron-sized bacterial detection system. (b) Photographs of the detection region in the fabricated microfluidic glass chip (scale bar = 100 μm). (c) Illustration of varing thickness of the detection area (gray) obtained by controlling the flow rate of the virtual wall (black).

3.3. Experimental Method

3.3.1. Sample Preparation

The author used fluorescent microparticles (0.99, 1.69, and 4.16 μm in diameter, Bangs Laboratory) to examine the performance of the system and verify the effect of the movable virtual wall. The excitation and emission wavelengths of the microparticles were 488 nm and 520 nm, respectively. The microparticles were suspended in a high-conductivity solution (1M KCl or phosphate buffered saline (PBS), pH 7.4) before use. Toxin-inactivated bacteria *F. tularensis* were obtained from Korea Centers for Disease Control and Prevention (KCDC). *F. tularensis* was stained with anti-T14 (HyTest), followed by Alexa 610PE-conjugated secondary antibodies (Invitrogen). Bacteria BL21 (Invitrogen) were transformed with plasmids encoding enhanced green fluorescence protein (EGFP). Hexadecane (Sigma-Aldrich), a non-conducting and water-immiscible liquid, was used as a virtual wall solution.

3.3.2. Simulation

The effect of the movable virtual wall was examined by numerical simulation using COMSOL Multiphysics (ver. 4.3a, COMSOL Inc.). The current density (A m^{-2}) in the 2-D horizontal plane including the main channel (60 μm width) was solved with electrostatic conditions, applying a 1 V DC voltage to a pair of electrodes. A pair of PGEs placed at the main channel was regarded as a current passage. The electrical conductivity (σ) and permittivity (ε) of the sample solution were set as 1.6 S m^{-1} and 76, respectively. For the virtual wall solution, σ = 0.00001 S m^{-1} and ε = 2.2. Without the virtual wall, the channel was modeled when filled only with a buffer solution (Figure 3-4(a)), whereas with the virtual wall the channel was set to be filled with a buffer and a virtual wall solution (Figure 3-4(b)). The proportion of the virtual wall solution was arbitrarily set to 83 %.

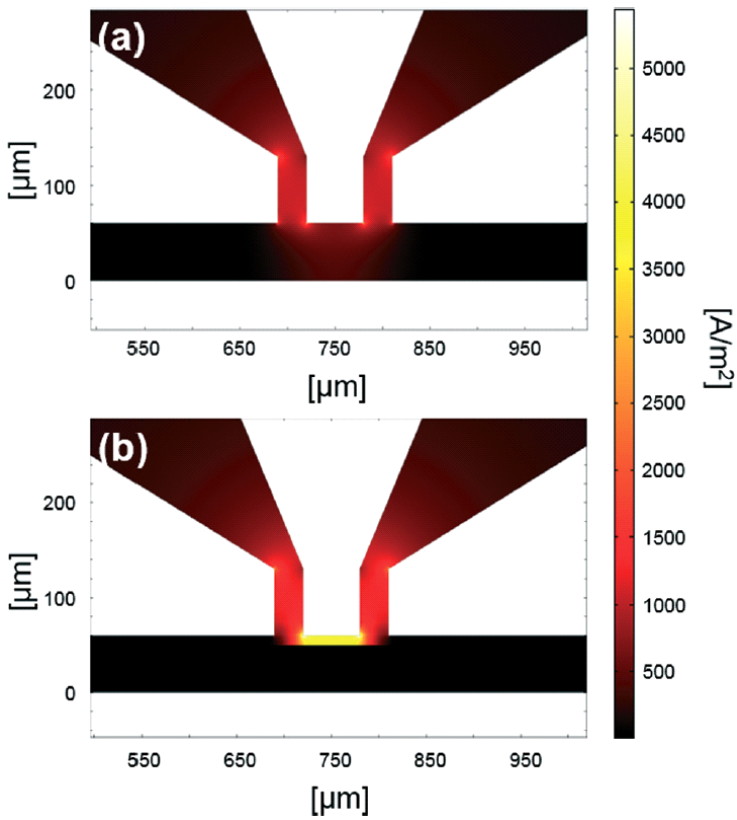

Figure 3-5. Simulation results of the current density (A m^{-2}) obtained by applying a 1 V DC voltage to a pair of electrodes (a) without and (b) with the virtual wall

3.3.3. Experimental Setup

For simultaneous detection of fluorescence and DC impedance change (ΔZ), fluorescent microparticles (0.99, 1.69, and 4.16 μm in diameter) dispersed in a high-conductivity solution were injected into the sample inlet at a flow rate of 1 μl min^{-1} while the non-conducting wall solution was pumped at a flow rate of 0.1, 0.3, 0.5, and 1 μl min^{-1} by syringe pumps (KD Scientific Inc.) to vary the effective channel width. The syringe tubes and sample inlets were connected by NanoPort assemblies (Upchurch). The width of the microfluidic channel was measured with MATLAB (The MathWorks, Inc.) using images captured with a T-2000 microscope (Nikon) equipped with a CV-S3200 CCD camera (Jai) and 20x objective lens (Nikon).

Changes in DC impedance were measured with a custom-made DC impedance detection circuit, based on those in previous reports [19, 97]. The circuit was designed to generate a constant DC voltage between two electrodes (0.8 V) and to calculate the derivatives of DC impedance signals in the detection region between the two PGEs.

The fluorescence detection system consisted of a light source

(488 nm, Ar laser), photomultiplier tube (PMT, Hamamatsu), and optical components such as an objective lens (40x, Nikon), dichroic mirror (Thorlabs), and fluorescence filters (520 nm and 610 nm) (Thorlabs). The battery-driven PMT control board was built upon a custom-made circuit. Output signals of the DC impedance and PMT control circuit were transmitted through a data acquisition card (National Instruments) at a 10 kHz sampling rate. The transmitted signals were then filtered to remove low frequency and 60 Hz noise, displayed, and saved using LabView software (National Instruments).

3.4. Results & Discussion

3.4.1. Simulation

The author performed numerical experiments to understand the effect of the virtual wall on current density. Figure 3-4 shows the distribution of the current density around the PGEs including the horizontal plane of the main channel. Without the virtual wall, the ionic currents spread throughout the entire main channel, yielding a low current density (~800 A m^{-2}) (Figure 3-4(a)). In contrast, with the virtual wall, the ionic current is contained within the conductive

buffer solution, yielding greater current density (~4000 A m^{-2}) (Figure 3-4(b)). The simulation results correspond to our experimental observations in which the virtual wall system indeed enhanced the sensitivity for detection of submicron particles (vide infra).

3.4.2. Detection of Changes in DC impedance and Fluorescence

At first, the author used a sample solution containing 4.16 μm microparticles at flow rates of 1 and 0.5 μl min^{-1} for the sample and virtual wall solutions, respectively. The signals (ΔZ) coming from the spots in front of the PGEs correspond to the derivatives of the DC impedance, in that an upward peak appeared as DC impedance increased when a particle entered the electric field. Likewise, a downward impedance peak with the same amplitude was observed when the particle left the electric field (Figure 3-5). Because the excitation laser was focused in between the two PGEs, the fluorescence signal had a peak in between the biphasic ΔZ signals. We verified that every pair of biphasic ΔZ signals synchronized well with the single monophasic fluorescence signal.

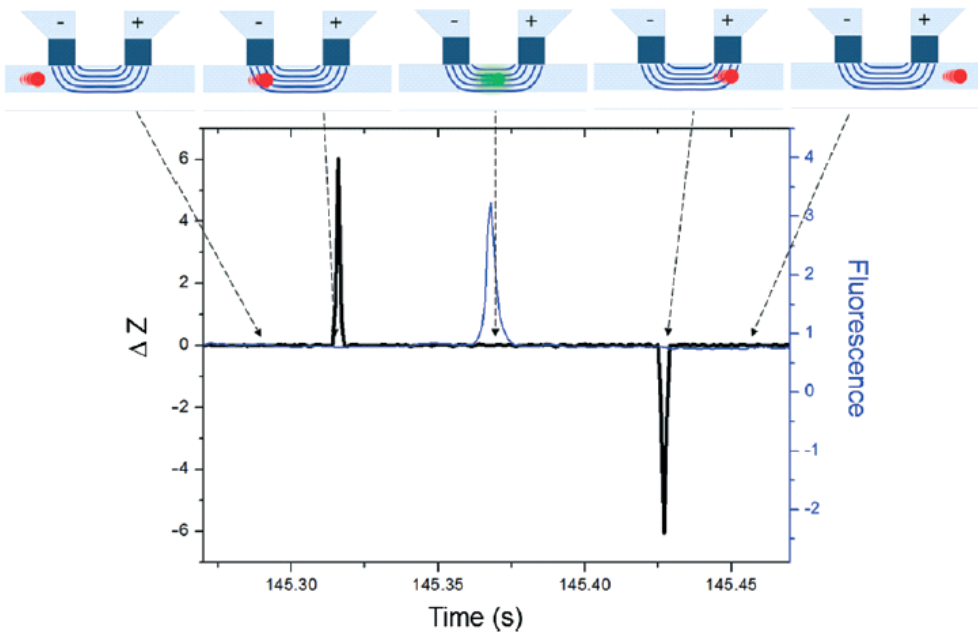

Figure 3-6. Representative profile of simultaneous detection of DC impedance changes (ΔZ) and fluorescence signals from 4.16 μm diameter polymer particles The fluorescence peak lies in between the biphasic ΔZ peaks.

3.4.3. Effect of the Movable Virtual Wall

According to the simulation results, the amplitude of the ΔZ signals should increase as the width of the channel where a major ionic current flow decreases. We first ensured that the channel width decreased as the flow rate of virtual wall solution increased (Figure 3-6). When we raised the flow rate of the virtual wall solution from 0.1 to 1 μl min^{-1} with a fixed sample solution flow rate (1 μl min^{-1}), the peak amplitudes of ΔZ signals originating from the 1.69 μm diameter microparticles increased from ~0.12 to ~1.0 (Figure 3-7). Figure 3-8(a) and (b) show typical simultaneous ΔZ and fluorescence signals when the flow rate of the virtual wall solution was 0.3 and 1 μl min^{-1}, respectively.

To examine the effect of particle size, we next used a different-sized set of fluorescent microparticles. When we fixed the flow rate of the virtual wall solution, the peak amplitude of ΔZ signals was proportional to the size of microparticles. Similarly, for a given size of microparticle, the peak amplitude of the ΔZ signals grew in commensurate with the flow rate of the virtual wall solution (Figure 3-8(c)). The channel width of the detection region was ~30 μm at the constant flow rate of the virtual wall solution of 0.1 μl

min^{-1} (see Figure 3-6). In this case, we could hardly detect 0.99 μm diameter microparticles owing to low sensitivity. However, at the higher flow rate of virtual wall solution, 1 μl min^{-1}, the submicron-sized microparticles produced sufficiently large ΔZ signals for quick and clear identification. These results proved that the sensitivity of our system is proportionally dependent upon the flow rate of the virtual wall solution. The values of the mean (m) and standard deviation (σ) of the peak amplitudes of ΔZ for three different types of microparticles are listed in Table 3-1.

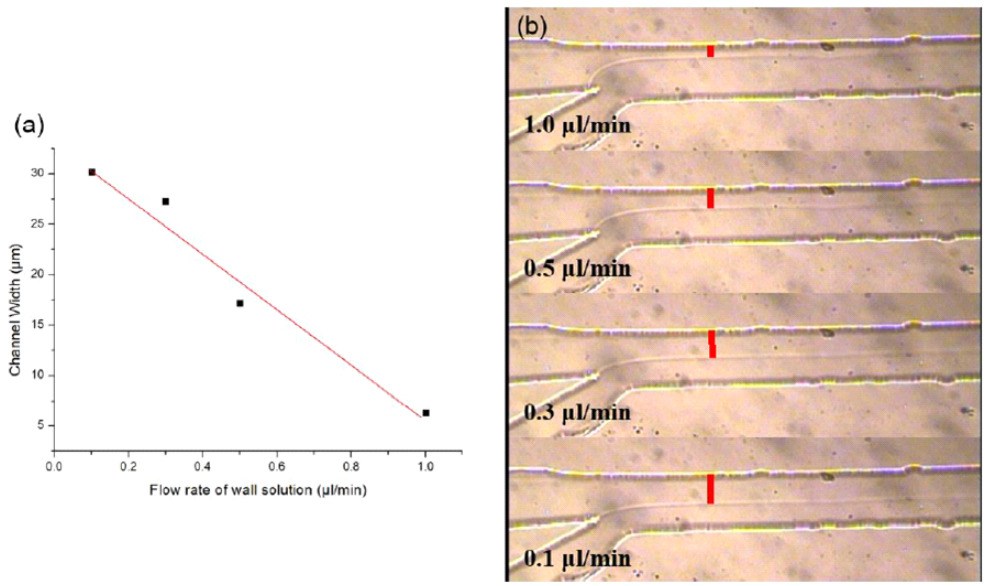

Figure 3-7. (a) The effective channel width as a function of the flow rate of virtual wall solution. The effective channel has only a high-conductivity solution, excluding the part of a low-conductivity wall solution (b) Photographs of the main microchannel in which the width of the effective channel (indicated by red lines) varies according to the flow rate of virtual wall solution (0.1, 0.3, 0.4, and 1 μl min^{-1}) with a fixed flow rate of a sample solution (1 μl min^{-1}).

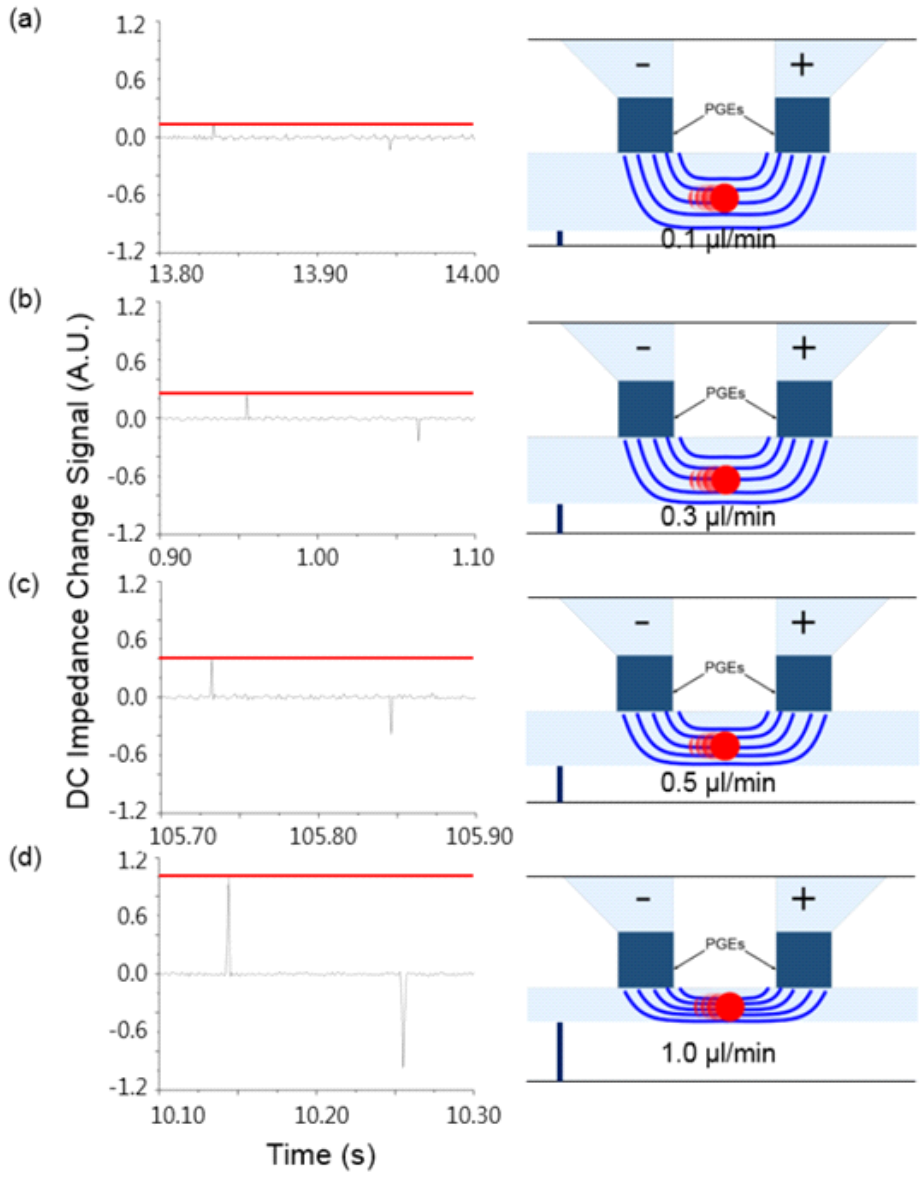

Figure 3-8. Examples of DC impedance signals (ΔZ) of 1.69 μm-sized microparticles according to the various flow rates of virtual wall solution: (a) 0.1, (b) 0.3, (c) 0.5, and (d) 1.0 μl min^{-1}. With a

constant size of microparticle, the amplitude of the ΔZ signals varies as a function of the flow rate of the virtual wall solution. Higher flow rate of the virtual wall solution (indicated by nave blue lines) leads to a smaller detection volume. As the detection volume is reduced, ionic flows are perturbed more by the same-sized microparticles, which gives rise to greater amplitudes of the ΔZ signals (red lines).

Table 3-1. The values of the mean (m) and standard deviation (σ) of the ΔZ signal peak amplitudes from various microparticles (0.99, 1.69, and 4.16 μm in diameter) according to the flow rate of the virtual wall solution (0.1, 0.3, 0.5, and 1 μl min^{-1}). ([a]nd = not determined)

Flow rate (μl min^{-1}) \ Diameter (μm)		0.99	1.69	4.16
0.1	m	nd[a]	0.121	1.80
	σ	nd[a]	0.0108	0.171
0.3	m	0.0500	0.249	3.71
	σ	0.00513	0.0203	0.324
0.5	m	0.0818	0.407	6.07
	σ	0.0109	0.0401	0.781
1.0	m	0.202	1.01	Saturated
	σ	0.0191	0.0843	Saturated

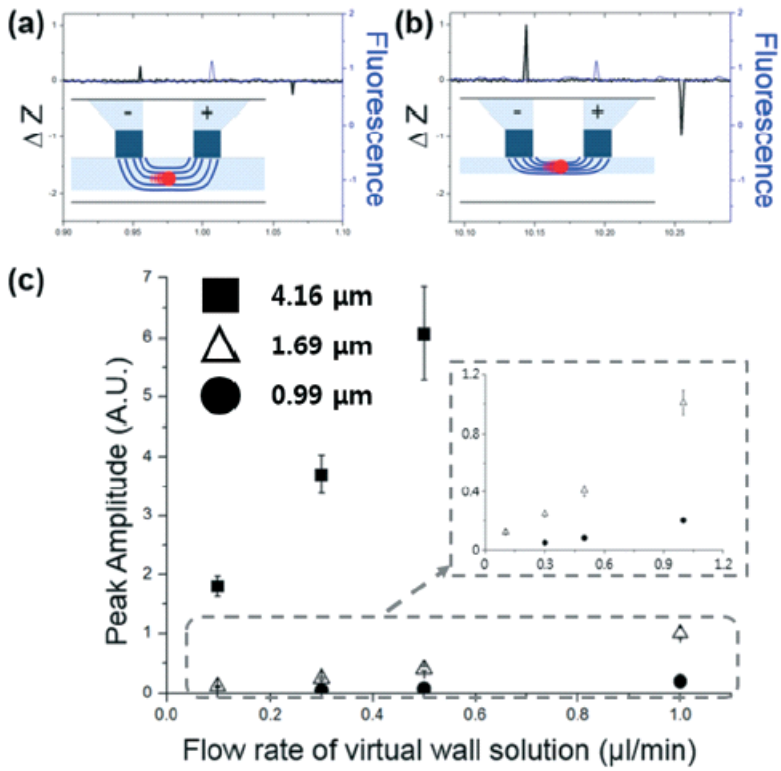

Figure 3-9. Representative simultaneous ΔZ and fluorescence signals from 1.69 μm diameter microparticles with different flow rates of virtual wall solution. The tiny ΔZ peaks significantly increase when the flow rate of the virtual wall solution changes from (a) 0.3 to (b) 1 μl min^{-1}, whereas the flow rate of the sample solution remains 1 μl min^{-1}. (c) The peak amplitudes of the ΔZ signals from microparticles (0.99, 1.69, and 4. 16 μm in diameter) increase as the flow rate of the virtual wall solution increases from 0.1 to 1 μl min^{-1} (n = 500).

3.4.4. Bacterial Detection

To apply the developed system for the detection of live bacteria, we chose the mixed samples of *F. tularensis* and *E. coli* BL21. The tularemia-causing *F. tularensis* is submicron-sized bacteria (0.4 to 0.7 μm in diameter) and is classified as a Class A Select Agent by the U.S. Department of Health and Human Services (HHS). Figure 3-9 shows one of the typically observed results of ΔZ and dual fluorescence signals. Two different types of ΔZ peaks, tall and short, were synchronized with green (520 nm) and red (610 nm) fluorescence signal peaks, respectively, at 1 μl min^{-1} of both the virtual wall and sample solutions (Figure 3-9(a)). The short peaks were from *F. tularensis* and the tall peaks from *E. coli*, as the *F. tularensis* was stained with Alexa 610PE dye and the E. coli was transformed with EGFP. The existence of the bacterium was ascertained from the position of the fluorescence signals in the middle of the upward and downward ΔZ peaks (Figure 3-9(a), gray box). The distribution profile and statistical values, including the means (m) and standard deviations (σ) of the peak amplitudes of the ΔZ signals, for two types of bacteria and two types of microparticles are shown in Figure 3-9(b) and Table 3-2.

To analyze the size distribution of the bacteria, we compared the ΔZ signals of *F. tularensis* and *E. coli* with those from the 0.99 and 1.69 μm diameter microparticles (Figure 3-10)). Based on the peak amplitudes of the ΔZ signals (see Figure 3-8(c)), we calculated the diameters of the bacteria on the assumption that the bacteria were spherical. The calculated diameters of *F. tularensis* were normally distributed with a mean (m) of 0.822 μm and a standard deviation (σ) of 0.0728 μm, which is mostly smaller than 1 μm (Table 3-3). The size of E. coli was relatively spread over a wide range, which included the diameters of the 1.69 μm microparticles. These results clearly show that the developed system could identify submicron-sized bacteria (~0.8 μm in average diameter) and differentiate them from several micron-sized bacteria.

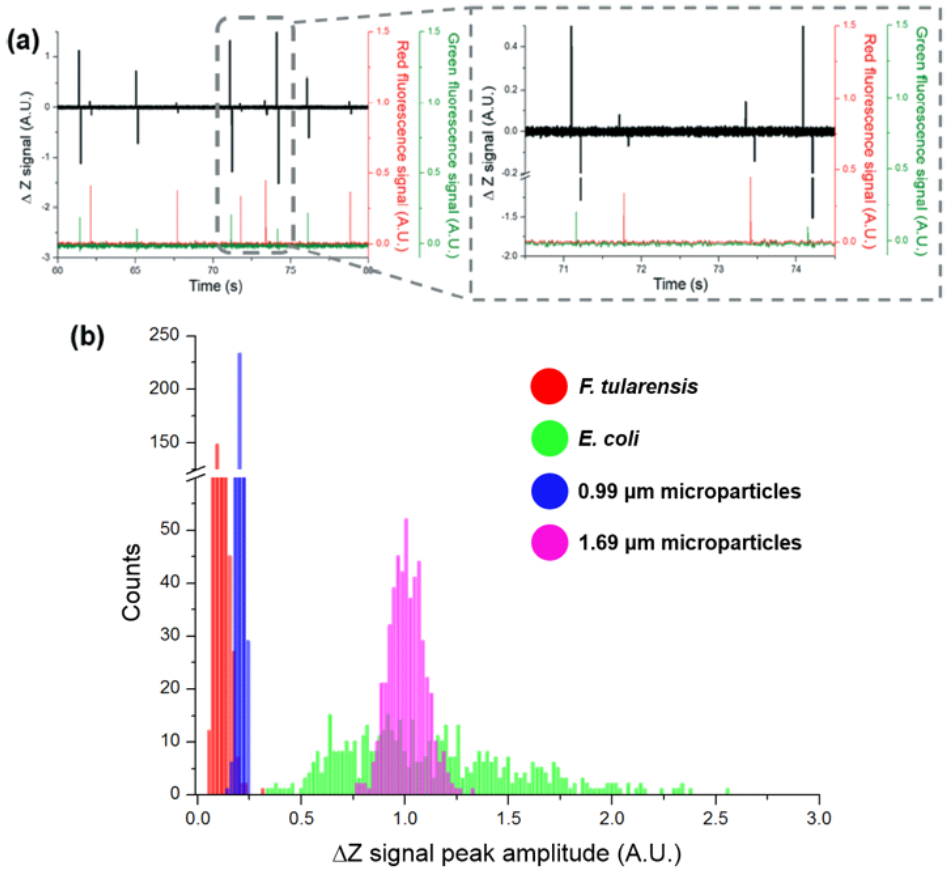

Figure 3-10. Detection of *F. tularensis*, *E. coli*, and two different types of microparticles. (a) representative DC impedance change (ΔZ) and fluorescence (520 and 610 nm) signals from a sample containing both *F. tularensis* and *E. coli*. The tall ΔZ peaks (green) and the short ΔZ peaks (red) synchronized with the green (520 nm) and the red (610 nm) fluorescence signals, respectively. (b) Distribution profile of the calculated diameters for *F. tularensis*, *E. coli*, and two types of microparticles (n = 500).

Table 3-2. The mean (m) and standard deviation (σ) values of peak amplitudes of the ΔZ signals of the tested samples (*F. tularensis, E. coli*, 0.99 and 1.69 μm in diameter). The flow rates of sample solution and virtual wall solution are fixed at 1 μl min^{-1}.

Samples / Peak amplitude (A.U.)	*F. tularensis*	0.99 μm microparticles	*E. coli*	1.69 μm microparticles
Mean *(m)*	0.119	0.202	1.12	1.00
Satandard deviation *(σ)*	0.0323	0.158	0.411	0.0848

Table 3-3. The mean (m) and standard deviation (σ) values of calculated diameters of the tested samples (*F. tularensis, E. coli*, 0.99 and 1.69 μm in diameter) from ΔZ peak amplitudes using flow cytometry-based bacterial detection system, assuming a spherical shape of the bacteria. The flow rates of sample solution and virtual wall solution are fixed at 1 μl min^{-1}.

Samples / Calculated diameter (μm)	*F. tularensis*	0.99 μm microparticles	*E. coli*	1.69 μm microparticles
Mean *(m)*	0.822	0.989	1.73	1.69
Satandard deviation *(σ)*	0.0728	0.0260	0.212	0.0477

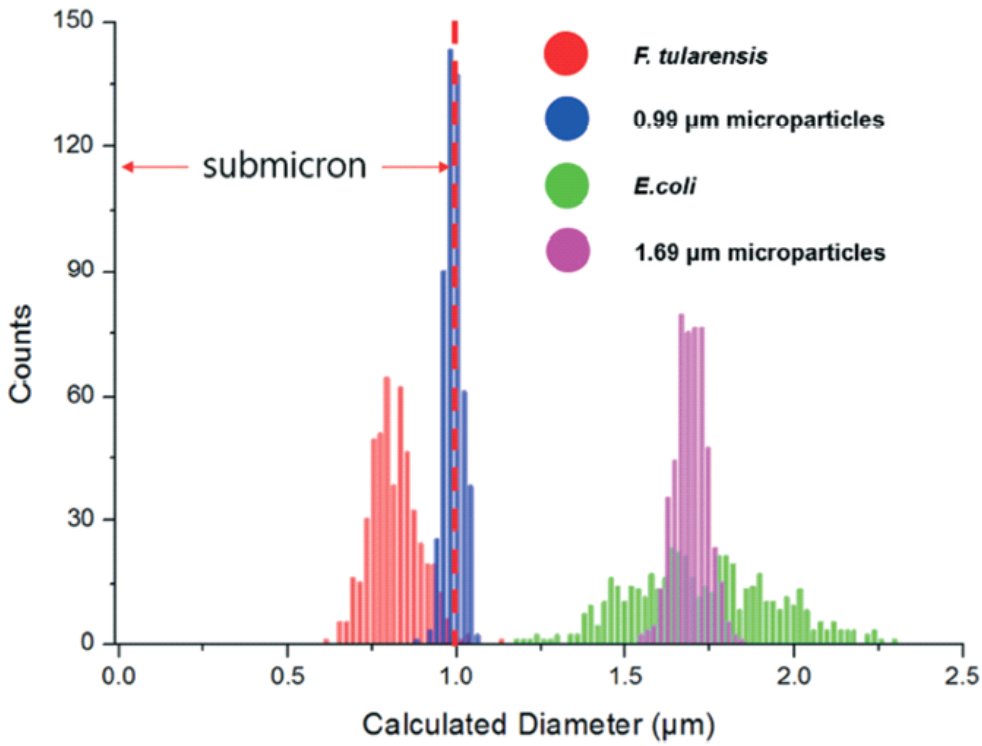

Figure 3-11. Distribution profile of the calculated diameters for *F. tularensis*, *E. coli*, and two different types of microparticles (n = 500).

3.5. Conclusion and Perspective

In this work, the author demonstrated that the proposed flow cytometry-based bacterial detection system could not only detect micron-sized particles and bacteria, but also distinguish them by simultaneously measuring DC impedance and multiple fluorescence signals. By introducing a movable virtual wall made of a non-conducting solution, we were able to finely adjust the effective channel width by controlling the flow rate of the wall solution. The experiments as well as the numerical simulations proved that the current density augmented as a result of narrowing the effective channel where the conductive sample solution flowed. Consequently, we successfully identified the submicron-sized bacteria, *F. tularensis* among various types of bacterial cells, indicating that the cytometry-based bacterial sensor developed in this study has a potential to be a fast, sensitive, accurate, and portable means of bacterial detection.

Publications

Hyoungseon Choi, Chang Su Jeon, Inseong Hwang, Juhui Ko, Saram Lee, Jaebum Choo, Jin-Hyo Boo, Hee Chan Kim and Taek Dong

Chung, "Flow Cytometry-based Submicron-sized Bacterial Detection System using Movable Virtual Wall", ***Lab on a Chip***, 2014, 14(13), 2327-2333.

Chapter 4.

Conclusion and Perspective

This dissertation is study of the miniaturization of flow cytometry system using microfluidic chip technologies and its applications which can be applied to our daily lives. Though there are several commercial flow cytometers which are small, well-made, and relatively affordable, more researches are needed for further reduction of expenses, complexity, and the size of flow cytometers. Thus, it is expected that microfluidics technology lead to effective flow cytometers for clinical POCT devices such as blood analysis and daily surrounding environment screening on site.

In this work, the author showed that i) the reasons why microfluidics integrated-flow cytometry system needed; small sample volume, simplicity, low-costs, portability, and unnecessity of operators, ii) an application to show the possibility for a daily healthcare device : a label-free DC impedance-based microcytometer to count circulating rare cancer cells, and iii) the other application to employ to water quality testing : a flow cytometry-based bacteria detection system using movable virtual wall.

Chapter 2 presents the definition of circulating tumor cell (CTC), the importance of the number of CTCs, and the approaches to detect CTCs. CTCs are detached cells from the primary tumor, having potential of metastasis to another organs. Thus, the number of

CTCs is highly-related to the patient's state. Among several approaches to detect CTCs, we chose a morphology-based method using size difference between CTCs and peripheral blood cells such as RBCs and WBCs. We successfully counted OVCAR-3 cancer cells spiked into 500 μl blood with 88 % detection efficiency. Furthermore, we obtained positive results from all of breast cancer patients' blood samples. For these reasons, the proposed microcytometer has a potential to be a portable and sensitive cancer diagnosis device at the site of patient care.

Chapter 3 shows the needs of fast and sensitive bacteria detection and the flow cytometry-based submicron-sized bacteria detection platform using adjustable virtual wall. By applying virtual wall with a non-conducting solution, the width of the effective channel where ions flow can be finely-adjusted to the size of targets. We proved the effect of non-conducting virtual wall with numerical simulation and experiments. Furthermore, submicron-sized bacteria, *F. tularensis*, were identified with the proposed platform and distinguished from mixed samples with *E. coli*. Therefore, the cytometry-based bacterial detection system developed in this chapter is a sensitive, accurate, and fast means of bacterial identification.

As shown in 2 chapters, microfluidics-based flow cytometry

system has numerous advantages in terms of portability, small sample volume, analysis time, costs, and sensitivity. Therefore, it is expected to be a portable and low-costs platform for small volume and sensitive analysis. However, there still remains lots of technologies need to be developed, because many on-chip platforms rely on large, expensive external devices. For instance, hydrodynamic focusing for cells to line up requires several high-precision syringe pumps or compressed-air-based pumps. In addition, optical detection system needs expensive and large optical components and light sources. Therefore, additional developments and improvements to help a microfluidic chip system for portability and low costs are necessary.

The author hope that with the peripheral instrument development, microfluidic chip-based miniaturized platform for clinical trials and biomedical researches, especially flow cytometry, keep growing and open a new market in this fields in the future.

Bibliography

[1] Lapsley, M. I.; Wang, L.; Huang, T. J., Biomarkers in Medicine 2013, 7 (1), 75-78.

[2] Hogg, W. R.; Hialeah, F.; Wallace H. Coulter, M. S., Fla. US Pat., 3,557,352, 1967.

[3] DeBlois, R. W.; Bean, C. P.; Wesley, R. K. A., Journal of Colloid And Interface Science 1977, 61 (2), 323-335.

[4] Ligler, F. S.; Kim, J. S., The Microflow Cytometer. Pan Stanford Publishing Pte. Ltd.: 2010.

[5] Fu, A. Y.; Chou, H. P.; Spence, C.; Arnold, F. H.; Quake, S. R., Analytical Chemistry 2002, 74 (11), 2451-2457.

[6] Tokeshi, M.; Kikutani, Y.; Hibara, A.; Sato, K.; Hisamoto, H.; Kitamori, T., Electrophoresis 2003, 24 (21), 3583-3594.

[7] Brown, M.; Wittwer, C., Clinical Chemistry 2000, 46 (8 II), 1221-1229.

[8] Maecker, H. T.; McCoy, J. P.; Nussenblatt, R., Nature Reviews Immunology 2012, 12 (3), 191-200.

[9] Huh, D.; Gu, W.; Kamotani, Y.; Grotberg, J. B.; Takayama, S., Physiological Measurement 2005, 26 (3), R73-R98.

[10] Ying, L.; Wang, Q., BMC Biotechnology 2013, 13.

[11] Joo, S.; Kim, K. H.; Kim, H. C.; Chung, T. D., Biosensors and Bioelectronics 2010, 25 (6), 1509-1515.

[12] Sims, C. E.; Allbritton, N. L., Lab on a Chip - Miniaturisation for Chemistry and Biology 2007, 7 (4), 423-440.

[13] Wolff, A.; Perch-Nielsen, I. R.; Larsen, U. D.; Friis, P.; Goranovic, G.; Poulsen, C. R.; Kutter, J. P.; Telleman, P., Lab on a Chip - Miniaturisation for Chemistry and Biology 2003, 3 (1), 22-27.

[14] Tung, Y. C.; Zhang, M.; Lin, C. T.; Kurabayashi, K.; Skerlos, S. J., Sensors and Actuators, B: Chemical 2004, 98 (2-3), 356-367.

[15] Watts, B. R.; Zhang, Z.; Xu, C. Q.; Cao, X.; Lin, M., Electrophoresis 2014, 35 (2-3), 271-281.

[16] Chung, T. D.; Kim, H. C., Electrophoresis 2007, 28 (24), 4511-4520.

[17] Gawad, S.; Schild, L.; Renaud, P., Lab on a Chip - Minituarization for Chemistry and Biology 2001, 1 (1), 76-82.

[18] Holmes, D.; Morgan, H., Analytical Chemistry 2010, 82 (4), 1455-1461.

[19] Chun, H.; Chung, T. D.; Kim, H. C., Analytical Chemistry

2005, 77 (8), 2490-2495.

[20] Barat, D.; Spencer, D.; Benazzi, G.; Mowlem, M. C.; Morgan, H., Lab on a Chip - Miniaturisation for Chemistry and Biology 2012, 12 (1), 118-126.

[21] Zieglschmid, V.; Hollmann, C.; B?cher, O., Critical Reviews in Clinical Laboratory Sciences 2005, 42 (2), 155-196.

[22] Miller, M. C.; Doyle, G. V.; Terstappen, L. W. M. M., Journal of Oncology 2010, 2010, 8 pages.

[23] Cohen, S. J.; Punt, C. J. A.; Iannotti, N.; Saidman, B. H.; Sabbath, K. D.; Gabrail, N. Y.; Picus, J.; Morse, M.; Mitchell, E.; Miller, M. C.; Doyle, G. V.; Tissing, H.; Terstappen, L. W. M. M.; Meropol, N. J., Journal of Clinical Oncology 2008, 26 (19), 3213-3221.

[24] He, W.; Kularatne, S. A.; Kalli, K. R.; Prendergast, F. G.; Amato, R. J.; Klee, G. G.; Hartmann, L. C.; Low, P. S., International Journal of Cancer 2008, 123 (8), 1968-1973.

[25] De Bono, J. S.; Scher, H. I.; Montgomery, R. B.; Parker, C.; Miller, M. C.; Tissing, H.; Doyle, G. V.; Terstappen, L. W. W. M.; Pienta, K. J.; Raghavan, D., Clinical Cancer Research 2008, 14 (19), 6302-6309.

[26] Paterlini-Brechot, P.; Benali, N. L., Cancer Letters 2007, 253

(2), 180-204.

[27] Osta, W. A.; Chen, Y.; Mikhitarian, K.; Mitas, M.; Salem, M.; Hannun, Y. A.; Cole, D. J.; Gillanders, W. E., Cancer Research 2004, 64 (16), 5818-5824.

[28] Baizar, M.; Winter, M. J.; De Boer, C. J.; Litvinov, S. V., Journal of Molecular Medicine 1999, 77 (10), 699-712.

[29] Pauli, C.; M?nz, M.; Kieu, C.; Mack, B.; Breinl, P.; Wollenberg, B.; Lang, S.; Zeidler, R.; Gires, O., Cancer Letters 2003, 193 (1), 25-32.

[30] Poczatek, R. B.; Myers, R. B.; Manne, U.; Oelschlager, D. K.; Weiss, H. L.; Bostwick, D. G.; Grizzle, W. E., Journal of Urology 1999, 162 (4), 1462-1466.

[31] Allard, W. J.; Matera, J.; Miller, M. C.; Repollet, M.; Connelly, M. C.; Rao, C.; Tibbe, A. G. J.; Uhr, J. W.; Terstappen, L. W. M. M., Clinical Cancer Research 2004, 10 (20), 6897-6904.

[32] Wan, Y.; Tan, J.; Asghar, W.; Kim, Y. T.; Liu, Y.; Iqbal, S. M., Journal of Physical Chemistry B 2011, 115 (47), 13891-13896.

[33] Herr, J. K.; Smith, J. E.; Medley, C. D.; Shangguan, D.; Tan, W., Analytical Chemistry 2006, 78 (9), 2918-2924.

[34] Kang, J. H.; Krause, S.; Tobin, H.; Mammoto, A.;

Kanapathipillai, M.; Ingber, D. E., Lab on a Chip - Miniaturisation for Chemistry and Biology 2012, 12 (12), 2175-2181.

[35] Myung, J. H.; Gajjar, K. A.; Saric, J.; Eddington, D. T.; Hong, S., Angewandte Chemie - International Edition 2011, 50 (49), 11769-11772.

[36] Fischer, A. H., Archives of Pathology and Laboratory Medicine 2009, 133 (9), 1367-1369.

[37] Riethdorf, S.; Fritsche, H.; M?ller, V.; Rau, T.; Schindlbeck, C.; Rack, B.; Janni, W.; Coith, C.; Beck, K.; J?nicke, F.; Jackson, S.; Gornet, T.; Cristofanilli, M.; Pantel, K., Clinical Cancer Research 2007, 13 (3), 920-928.

[38] Maheswaran, S.; Haber, D. A., Current Opinion in Genetics and Development 2010, 20 (1), 96-99.

[39] Vona, G.; Sabile, A.; Louha, M.; Sitruk, V.; Romana, S.; Schutze, K.; Capron, F.; Franco, D.; Pazzagli, M.; Vekemans, M.; Lacour, B.; Brechot, C.; Paterlini-Brechot, P., American Journal of Pathology 2000, 156 (1), 57-63.

[40] Lara, O.; Tong, X.; Zborowski, M.; Chalmers, J. J., Experimental Hematology 2004, 32 (10), 891-904.

[41] Lin, H. K.; Zheng, S.; Williams, A. J.; Balic, M.; Groshen, S.;

Scher, H. I.; Fleisher, M.; Stadler, W.; Datar, R. H.; Tai, Y. C.; Cote, R. J., Clinical Cancer Research 2010, 16 (20), 5011-5018.

[42] Desitter, I.; Guerrouahen, B. S.; Benali-Furet, N.; Wechsler, J.; J?nne, P. A.; Kuang, Y.; Yanagita, M.; Wang, L.; Berkowitz, J. A.; Distel, R. J.; Cayre, Y. E., Anticancer Research 2011, 31 (2), 427-441.

[43] Rosenberg, R.; Gertler, R.; Friederichs, J.; Fuehrer, K.; Dahm, M.; Phelps, R.; Thorban, S.; Nekarda, H.; Siewert, J. R., Cytometry 2002, 49 (4), 150-158. DOI 10.1002/cyto.10161.

[44] Gertler, R.; Rosenberg, R.; Fuehrer, K.; Dahm, M.; Nekarda, H.; Siewert, J. R., Recent results in cancer research. Fortschritte der Krebsforschung. Progres dans les recherches sur le cancer 2003, 162, 149-155.

[45] Busch, R.; Cesar, D.; Higuera-Alhino, D.; Gee, T.; Hellerstein, M. K.; McCune, J. M., Journal of Immunological Methods 2004, 286 (1-2), 97-109.

[46] Hayes, G. M.; Busch, R.; Voogt, J.; Siah, I. M.; Gee, T. A.; Hellerstein, M. K.; Chiorazzi, N.; Rai, K. R.; Murphy, E. J., Leukemia Research 2010, 34 (6), 809-815.

[47] Nagrath, S.; Sequist, L. V.; Maheswaran, S.; Bell, D. W.;

Irimia, D.; Ulkus, L.; Smith, M. R.; Kwak, E. L.; Digumarthy, S.; Muzikansky, A.; Ryan, P.; Balis, U. J.; Tompkins, R. G.; Haber, D. A.; Toner, M., Nature 2007, 450 (7173), 1235-1239.

[48] Stott, S. L.; Hsu, C. H.; Tsukrov, D. I.; Yu, M.; Miyamoto, D. T.; Waltman, B. A.; Michael Rothenberg, S.; Shah, A. M.; Smas, M. E.; Korir, G. K.; Floyd Jr, F. P.; Gilman, A. J.; Lord, J. B.; Winokur, D.; Springer, S.; Irimia, D.; Nagrath, S.; Sequist, L. V.; Lee, R. J.; Isselbacher, K. J.; Maheswaran, S.; Haber, D. A.; Toner, M., Proceedings of the National Academy of Sciences of the United States of America 2010, 107 (43), 18392-18397.

[49] Lee, J. M.; Dedhar, S.; Kalluri, R.; Thompson, E. W., Journal of Cell Biology 2006, 172 (7), 973-981.

[50] Thompson, E. W.; Newgreen, D. F., Cancer Research 2005, 65 (14), 5991-5995.

[51] Their, J. P., Nature Reviews Cancer 2002, 2 (6), 442-454.

[52] Steinarsd?ttir, M.; J?nasson, J. G.; Viorsson, H.; J?l?usd?ttir, H.; Hauksd?ttir, H.; ?gmundsd?ttir, H. M., Genes Chromosomes and Cancer 2004, 41 (1), 47-55.

[53] Sleijfer, S.; Gratama, J. W.; Sieuwerts, A. M.; Kraan, J.; Martens, J. W. M.; Foekens, J. A., European Journal of

Cancer 2007, 43 (18), 2645-2650.

[54] Jung, R.; Kr?ger, W.; Hosch, S.; Holweg, M.; Kr?ger, N.; Gutensohn, K.; Wagener, C.; Neumaier, M.; Zander, A. R., British Journal of Cancer 1998, 78 (9), 1194-1198.

[55] Cristofanilli, M.; Budd, G. T.; Ellis, M. J.; Stopeck, A.; Matera, J.; Miller, M. C.; Reuben, J. M.; Doyle, G. V.; Allard, W. J.; Terstappen, L. W. M. M.; Hayes, D. F., New England Journal of Medicine 2004, 351 (8), 781-791.

[56] Mohamed, H.; McCurdy, L. D.; Szarowski, D. H.; Duva, S.; Turner, J. N.; Caggana, M., IEEE Transactions on Nanobioscience 2004, 3 (4), 251-256.

[57] Mohamed, H.; Murray, M.; Turner, J. N.; Caggana, M., Journal of Chromatography A 2009, 1216 (47), 8289-8295.

[58] MacH, A. J.; Kim, J. H.; Arshi, A.; Hur, S. C.; Di Carlo, D., Lab on a Chip - Miniaturisation for Chemistry and Biology 2011, 11 (17), 2827-2834.

[59] Augustsson, P.; Magnusson, C.; Nordin, M.; Lilja, H.; Laurell, T., Analytical Chemistry 2012, 84 (18), 7954-7962.

[60] Hosokawa, M.; Hayata, T.; Fukuda, Y.; Arakaki, A.; Yoshino, T.; Tanaka, T.; Matsunaga, T., Analytical Chemistry 2010, 82 (15), 6629-6635.

[61] Zheng, S.; Lin, H.; Liu, J. Q.; Balic, M.; Datar, R.; Cote, R. J.; Tai, Y. C., Journal of Chromatography A 2007, 1162 (2 SPEC. ISS.), 154-161.

[62] Zheng, S.; Lin, H. K.; Lu, B.; Williams, A.; Datar, R.; Cote, R. J.; Tai, Y. C., Biomedical Microdevices 2011, 13 (1), 203-213.

[63] Tan, S. J.; Yobas, L.; Lee, G. Y. H.; Ong, C. N.; Lim, C. T., Biomedical Microdevices 2009, 11 (4), 883-892.

[64] Kim, M. S.; Sim, T. S.; Kim, Y. J.; Kim, S. S.; Jeong, H.; Park, J. M.; Moon, H. S.; Kim, S. I.; Gurel, O.; Lee, S. S.; Lee, J. G.; Park, J. C., Lab on a Chip - Miniaturisation for Chemistry and Biology 2012, 12 (16), 2874-2880.

[65] Lundahl, J.; Halld?n, G.; Hallgren, M.; Sk?ld, C. M.; Hed, J., Journal of Immunological Methods 1995, 180 (1), 93-100.

[66] Fukuda, S.; Schmid-Sch?nbein, G. W., Journal of Leukocyte Biology 2002, 72 (1), 133-139.

[67] Bhagat, A. A. S.; Hou, H. W.; Li, L. D.; Lim, C. T.; Han, J., Lab on a Chip - Miniaturisation for Chemistry and Biology 2011, 11 (11), 1870-1878.

[68] Park, J. S.; Jung, H. I., Analytical Chemistry 2009, 81 (20), 8280-8288.

[69] Park, J. S.; Song, S. H.; Jung, H. I., Lab on a Chip -

Miniaturisation for Chemistry and Biology 2009, 9 (7), 939-948.

[70] Moon, H. S.; Kwon, K.; Kim, S. I.; Han, H.; Sohn, J.; Lee, S.; Jung, H. I., Lab on a Chip - Miniaturisation for Chemistry and Biology 2011, 11 (6), 1118-1125.

[71] Adams, A. A.; Okagbare, P. I.; Feng, J.; Hupert, M. L.; Patterson, D.; G?tten, J.; McCarley, R. L.; Nikitopoulos, D.; Murphy, M. C.; Soper, S. A., Journal of the American Chemical Society 2008, 130 (27), 8633-8641.

[72] Dharmasiri, U.; Njoroge, S. K.; Witek, M. A.; Adebiyi, M. G.; Kamande, J. W.; Hupert, M. L.; Barany, F.; Soper, S. A., Analytical Chemistry 2011, 83 (6), 2301-2309.

[73] Kim, K. B.; Chun, H.; Kim, H. C.; Chung, T. D., Electrophoresis 2009, 30 (9), 1464-1469.

[74] Sun, T.; Morgan, H., Microfluidics and Nanofluidics 2010, 8 (4), 423-443.

[75] Holmes, D.; Pettigrew, D.; Reccius, C. H.; Gwyer, J. D.; Van Berkel, C.; Holloway, J.; Davies, D. E.; Morgan, H., Lab on a Chip - Miniaturisation for Chemistry and Biology 2009, 9 (20), 2881-2889.

[76] Purves, W. K.; Savada, D.; Orians, G. H.; Heller, H. C., Life:

The Science of Biology, 7th Edition. Sinauer Associates: 2003.

[77] Yu, M.; Stott, S.; Toner, M.; Maheswaran, S.; Haber, D. A., Journal of Cell Biology 2011, 192 (3), 373-382.

[78] Yoon, H. J.; Kim, T. H.; Zhang, Z.; Azizi, E.; Pham, T. M.; Paoletti, C.; Lin, J.; Ramnath, N.; Wicha, M. S.; Hayes, D. F.; Simeone, D. M.; Nagrath, S., Nature Nanotechnology 2013, 8 (10), 735-741.

[79] Xie, M.; Lu, N. N.; Cheng, S. B.; Wang, X. Y.; Wang, M.; Guo, S.; Wen, C. Y.; Hu, J.; Pang, D. W.; Huang, W. H., Analytical Chemistry 2014, 86 (9), 4618-4626.

[80] Whitman, W. B.; Coleman, D. C.; Wiebe, W. J., Proceedings of the National Academy of Sciences of the United States of America 1998, 95 (12), 6578-6583.

[81] Ivnitski, D.; Abdel-Hamid, I.; Atanasov, P.; Wilkins, E., Biosensors and Bioelectronics 1999, 14 (7), 599-624.

[82] McNamara, A. M., Journal of Urban Health 1998, 75 (3), 503-505.

[83] Slutsker, L.; Altekruse, S. F.; Swerdlow, D. L., Infectious Disease Clinics of North America 1998, 12 (1), 199-216.

[84] Velusamy, V.; Arshak, K.; Korostynska, O.; Oliwa, K.; Adley, C., Biotechnology Advances 2010, 28 (2), 232-254.

[85] Mayr, U. B.; Haller, C.; Haidinger, W.; Atrasheuskaya, A.; Bukin, E.; Lubitz, W.; Ignatyev, G., Infection and Immunity 2005, 73 (8), 4810-4817.

[86] Wang, S.; Inci, F.; Chaunzwa, T. L.; Ramanujam, A.; Vasudevan, A.; Subramanian, S.; Fai Ip, A. C.; Sridharan, B.; Gurkan, U. A.; Demirci, U., International Journal of Nanomedicine 2012, 7, 2591-2600.

[87] Meng, J.; Zhao, S.; Doyle, M. P.; Mitchell, S. E.; Kresovich, S., International Journal of Food Microbiology 1996, 32 (1-2), 103-113.

[88] Yamamoto, Y., Clinical and Diagnostic Laboratory Immunology 2002, 9 (3), 508-514.

[89] Dezenclos, T.; Ascon-Cabrera, M.; Ascon, D.; Lebeault, J. M.; Pauss, A., Applied Microbiology and Biotechnology 1994, 42 (2-3), 232-238.

[90] Watts, H. J.; Lowe, C. R.; Pollard-Knight, D. V., Analytical Chemistry 1994, 66 (15), 2465-2468.

[91] Schneider, B. H.; Edwards, J. G.; Hartman, N. F., Clinical Chemistry 1997, 43 (9), 1757-1763.

[92] Song, J. M.; Culha, M.; Kasili, P. M.; Griffin, G. D.; Vo-Dinh, T., Biosensors and Bioelectronics 2005, 20 (11), 2203-2209.

[93] Laczka, O.; Maesa, J. M.; Godino, N.; del Campo, J.; Fougt-Hansen, M.; Kutter, J. P.; Snakenborg, D.; Mu?oz-Pascual, F. X.; Baldrich, E., Biosensors and Bioelectronics 2011, 26 (8), 3633-3640.

[94] Attfield, P.; Gunasekera, T.; Boyd, A.; Deere, D.; Veal, D., Australasian Biotechnology 1999, 9 (3), 159-166.

[95] Karo, O.; Wahl, A.; Nicol, S. B.; Brachert, J.; Lambrecht, B.; Spengler, H. P.; Nauwelaers, F.; Schmidt, M.; Schneider, C. K.; Muller, T. H.; Montag, T., Clinical chemistry and laboratory medicine : CCLM / FESCC 2008, 46 (7), 947-953.

[96] Gunasekera, T. S.; Attfield, P. V.; Veal, D. A., Applied and Environmental Microbiology 2000, 66 (3), 1228-1232.

[97] Kim, J.; Kim, E. G.; Bae, S.; Kwon, S.; Chun, H., Analytical Chemistry 2013, 85 (1), 362-368.

[98] Bernabini, C.; Holmes, D.; Morgan, H., Lab on a Chip - Miniaturisation for Chemistry and Biology 2011, 11 (3), 407-412.

[99] Fraikin, J. L.; Teesalu, T.; McKenney, C. M.; Ruoslahti, E.; Cleland, A. N., Nature Nanotechnology 2011, 6 (5), 308-313.

[100] Choi, H.; Kim, K. B.; Jeon, C. S.; Hwang, I.; Lee, S.; Kim, H. K.; Kim, H. C.; Chung, T. D., Lab on a Chip -

Miniaturisation for Chemistry and Biology 2013, 13 (5), 970-977.

Appendix.

A. Chip Fabrication

A microfluidic glass chip was fabricated by similar photolithographic techniques in our previous reports [19]. Slide glasses (Marienfeld Laboratory Glassware) was put in piranha solution (H_2SO_4 : H_2O_2 = 1:3) for 45min, then cleaned with deionized (DI) water , acetone (CMOS grade, J. T. Baker), and methanol (CMOS grade, J. T. Baker) three times. Cleaned slide glasses were spin-coated (Won Corp.) with HMDS (hexamethyldisilazane) (Clariant) with 6,000 rpm for 30 sec. The HMDS-coated slide glass was placed on a hot plate at 150°C for 3 min and subsequently cooled at room temperature for 90 sec. Afterwards, the photoresist (PR) of AZ4620 (Clariant) coated the surface of the slide glass using spin coater at 6,000 rpm for 30 sec. After soft baking the PR-coated slide glass at 100°C for 90 sec, the slide glass was cooled at room temperature for 90 sec immediately. Then, the slide glass was aligned under a pattern-designed film mask (accumax photoplotter film, Kodak), and exposed to UV light (365 nm) for 13 sec with a UV aligner (Midas System Co., Ltd.). The UV-exposed slide glass was immersed into the AZ 400K developer (Clariant) for developing UV-exposed PR.

The slide glass was then washed with DI water and dried with the clean air. Next, the slide glass was hard-baked on a 150°C for 15 min. After cooling at room temperature, the slide glass was etched for 30 min using 6:1 buffered oxide etch (BOE) solution (J. T. Baker) and cleaned with DI water using an ultrasonic cleaner (351OE-DTH, Branson) for 15 min to remove impurities on the channel. The cover slide glass was drilled on inlet/outlet reservoirs and holes. The treated slide glass and drilled cover slide glass were cleaned in piranha solution. Then, two slide glasses were bonded thermally at 600°C for 5 h in a furnace (CRF-M15, CEBER). PGEs were constructed inside the bonded glass chip channels.

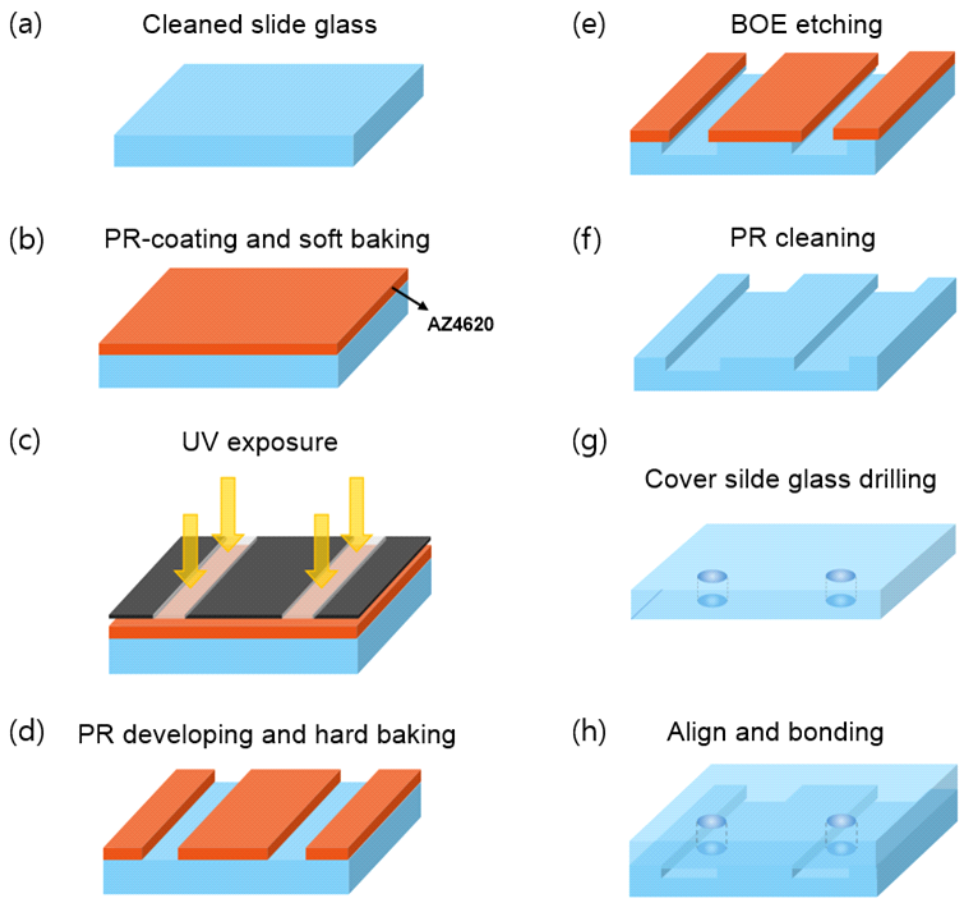

Figure Appendix 1. Chip fabrication processes. (a)-(f) Microchannel -patterned bottom glass using photolithography. (g) Top glass with holes. (h) Bonding between top and bottom glasses.

B. Polyelectrolytic Gel Electrode (PGE) Fabrication

The PGEs were fabricated by photopolymerization technique with our previous researches [19]. The surfaces of channels were coated with TMSMA (3-(trimethoxysilyl) propyl methacrylate) (Sigma-Aldrich) to enhance adhesion of PGEs. The monomer solution consisted of DADMAC (diallyldimethylammonium chloride) (Sigma-Aldrich), 2 % photoinitiator (2-hydroxy-40-(2-hydroxyethoxy)-2-methylpropiophenone) (Sigma-Aldrich) and 2 % cross-linker (N,N′-methylene-bisacrylamide) (Sigma-Aldrich). The microfluidic channels were filled with the monomer solution, and aligned under masking film. The desired position in channel was exposed with UV light (365 nm) and monomer solution in the desired position was polymerized. The microfluidic channel was cleaned and filled with 1 M KCl.

C. System parallelization plan

Multi-channel system comprised of 6-channel microfluidic chip and integrated circuit for 6 impedance and 6 fluorescence detection system. As shown in Figure Appendix 2(a), a microfluidic chip has one sample inlet, 6 sample outlets, and 6 main channels. Each main channels has their own detection region between PGEs. The customized circuit and system are connected to a microfluidic chip with 6 optical fibers and electrical wires.

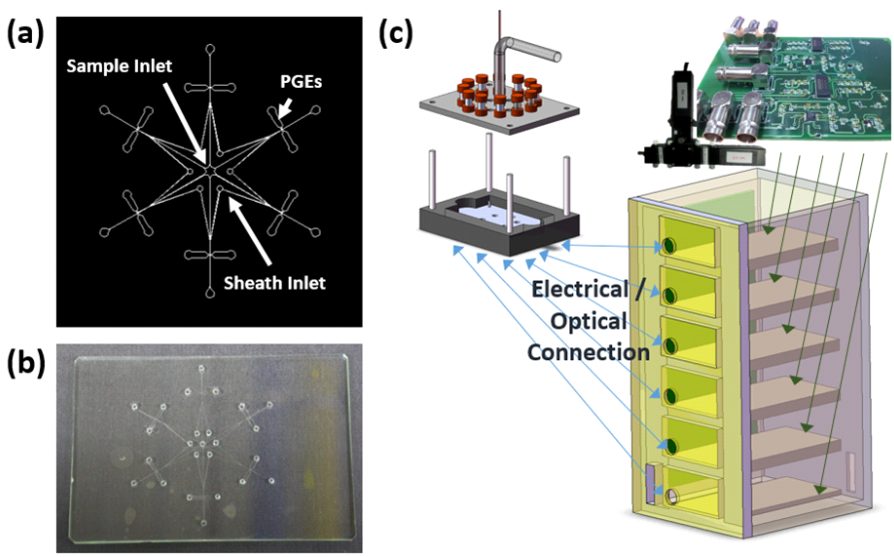

Figure Appendix 2. 6 Multi-channel system. (a) Mask pattern of the 6-channel microfluidic chip. (b) Photographs of the fabricated microfluidic chip. (c) Illustration of 6 multi-channel system with microfluidic chip holder and customized circuit.

국 문 초 록

본 논문은 미세유체 칩을 기반으로 한 소형화된 유동 세포 계수기 플랫폼과 그를 이용한 실용적 적용에 관한 연구이다. 유동세포 계수기는 세포 혹은 입자들의 여러 가지 특징들을 분석하고, 계수를 하기 위해서 전통적으로 많이 사용되어 온 기술이다. 임상학분야와 의공학 분야에서 유동세포 계수기의 POCT 기기로서의 필요성이 증가함에 따라, 값싸고 운용이 쉬운 소형화된 유동세포계수기의 개발이 전 세계적으로 행해지고 있다. 특히, 미세공정 기술 혁신과 함께 미세유체 시스템 기반의 유동세포 계수기 플랫폼을 생화학, 나노공학, 생물학, 기계공학, 전자공학에 걸친 여러 분야에 걸쳐서 필요로 하고 있다. 그 이유로는 적은 양의 시료 사용, 적은 비용, 작은 시스템 크기, 빠른 분석 시간으로 들 수 있다. 본 연구에서는 개발된 DC 임피던스 기반의 소형 유동세포계수기를 순환 암세포(CTC) 계수기와 박테리아 검출에 사용되는 활용에 대해서 보여줄 것이다.

첫째, CTC 검출을 위해서 간단하고, 라벨프리이며 효과적인 DC 임피던스 기반의 소형화된 계수기를 개발하였다. 순환 암세포 검출에는 여러 가지 방법이 사용되고 있지만, 대부분의 방법은 epithelial cell adhesion molecule (EpCAM)을 사용하는 면역분석 방법을 기반으로 한다. 하지만, 최근의 연구에서 EpCAM 이 epithelial-mesenchymal transition (EMT) 과정 중에 없어진다는 보고가 있었고, 일부 백혈구에

서 EpCAM 이 검출된다는 보고가 있었다. 그렇기 때문에, 본 연구에서는 CTC가 다른 백혈구나 적혈구보다 크기가 크다는 CTC 의 형태학적인 특징을 이용하여 시스템을 개발하였다. 개발된 DC 임피던스 유동세포계수기는 DC 임피던스 피크 크기를 이용하여 빠르게 지나가는 세포들의 크기를 측정하였다. 개발된 시스템을 이용하여, 88 % 효율로 난소암 세포를 계수하였고, 모든 유방암환자의 혈액에서 유의미한 개수의 CTC를 검출하였다. 이러한 결과들을 토대로 개발된 기기는 미래에는 휴대가 가능한 일상생활에서의 암진단 관련 건강관리 기기로 사용 될 수 있을 것으로 보인다.

둘째로 움직이는 가상의 벽을 이용한 유동세포 계수기 기반의 서브마이크론 크기의 박테리아 검출 시스템을 개발하였다. 수질을 검사하기 위해서 많은 종류의 박테리아 검출 방법이 사용되고 있다. 하지만, 전통적으로 사용되는 방법은 노동력이 많이 들고, 시간 소모가 24시간 이상으로 크다. 게다가 검사를 위해서 교육된 전문가가 필요로 하다는 단점이 있다. 이러한 한계들을 극복하기 위해서 비전도성 물질을 가상의 벽으로 활용하는 소형화된 유동세포 계수기 기반의 박테리아 검출 시스템을 개발하였다. 개발된 시스템은 기본적으로 DC 임피던스 검출을 이용하여 박테리아 크기를 측정하고 박테리아 존재 여부를 확인한다. 그리고 형광 검출을 이용하여 어떠한 종류의 박테리아 인지를 인지한다. 또한, 서브마이크론에서 4 마이크론미터 크기의 세포를 검출하기 위해서 비전도성 물질을 조절 가능한 가상의 벽으로 활용하였다. 가상의 벽 물질은

이온을 포함하지 않고, 층류로 형성되어 샘플 용액과 섞이지도 않기 때문에 채널의 벽처럼 여겨질 수 있다. 개발된 시스템을 이용하여 0.99, 1.69, 4.16 마이크론 미터 크기의 입자들과 서브마이크론 크기의 박테리아인 야토균을 검출하였다. 또한, 소형화된 계수기를 이용하여 야토균과 대장균을 DC 임피던스와 형광 검출을 이용하여 구별하는데 성공하였다. 이러한 결과들로부터, 개발된 유동세포 계수기 기반의 박테리아 검출기는 손쉽고, 민감하고, 정확하고 빠른 휴대용 박테리아 검출기로 사용될 수 있을 것으로 보인다.

주요어 : 미세유체 시스템, 유동 세포계수기, DC 임피던스 검출, 형광 검출, 순환 암세포 (CTC), 박테리아 검출

Student Number : 2009-21079